Evidence from U-Pb zircon geochronology for early Neoproterozoic (Tonian) reworking of an Archaean inlier in northeastern Shetland, Scottish Caledonides

I. Jahn[1*], R.A. Strachan [2], M. Fowler [2], E. Bruand. [2] P.D. Kinny[1], C. Clark [1] and R.J.M Taylor[1]

[1]*The Institute for Geoscience Research (TIGeR), Department of Applied Geology, Curtin University of Technology, GPO Box 1987, Perth, WA 6845, Australia*

[2]*School of Earth & Environmental Sciences, University of Portsmouth, Burnaby Road, Portsmouth PO1 3QL, UK*

**Correspondence (inalee.jahn@postgrad.curtin.edu.au)*

Abstract: Meta-igneous lithologies of the Cullivoe inlier in northeast Yell, Shetland, have TTG chemistry and yield U-Pb zircon crystallisation ages of *c.* 2856-2699 Ma. Formation was coeval with protoliths of the Lewisian Gneiss Complex and the time of major Neoarchaean crustal growth in the North Atlantic Craton. The adjacent metasedimentary Yell Sound Group accumulated between *c.* 1019 Ma and *c.* 941 Ma. The Cullivoe inlier and the Yell Sound Group together were metamorphosed at *c.* 944-931 Ma, the former preserving granulite facies mineral assemblages inferred to be of this age. Similar-aged metamorphic events recorded in other Laurentian metasedimentary successions in the North Atlantic region are attributed to development of the Valhalla orogen along the Rodinia margin. Ordovician (482 ± 30 Ma) and Silurian (428 ± 16 Ma) thermal rejuvenation resulted from successive phases of the Caledonian orogeny during closure of the Iapetus Ocean. The mechanism by which the Cullivoe inlier was emplaced into its current structural setting is uncertain. Either its western or eastern boundary is a major tectonic break, probably an early ductile thrust. However, this is now cryptic as a result of the Caledonian ductile reworking.

Supplementary material: SIMS and LA-ICP-MS analytical data, statistical analyses, and major trace element analytical data are available at

Central problems associated with high-grade, polymetamorphic terrains include the distinction between basement and cover units, in situations where ductile deformation has removed all traces of original depositional unconformities, and the identification of early tectonothermal events that may have been masked by subsequent reworking and mineral growth. In such terrains, U-Pb geochronology carried out on accessory minerals such as zircon, monazite and rutile is a key tool for constraining protolith ages and metamorphic events and hence resolving these issues. The Ordovician-Silurian Caledonian orogenic belt

(Fig. 1) is classic ground for the investigation of high-grade, polymetamorphic terrains. Caledonian orogenesis resulted from the closure of the Iapetus Ocean and collision of three continental blocks, Laurentia, Baltica and Avalonia (e.g. Pickering *et al.* 1988; Soper *et al.* 1992; Leslie *et al.* 2008). Despite widespread and often intense Caledonian reworking at amphibolite facies, modern geochronological and metamorphic investigations have made significant advances in distinguishing between basement and cover sequences and understanding the complex Precambrian tectonic evolution of the Laurentian-derived Northern Highland Terrane in Scotland (Fig. 1) (e.g. Rogers *et al.* 1998; Vance *et al.* 1998; Friend *et al.* 2008; Storey, 2008; Cutts *et al.* 2009, 2010; Cawood *et al.* 2010, 2015).

Shetland (Fig. 1) occupies a key location within the Caledonian orogenic belt due to its pre-Mesozoic proximity to the East Greenland, Scottish, and Norwegian sectors of the orogen. The pre-Devonian geology is dominated by orthogneiss complexes and metasedimentary successions which have been compared on lithological and geochemical grounds with various geological units in the Northern Highland and Grampian terranes of mainland Scotland (Flinn *et al.* 1972, 1979, Flinn 1985, 1988). However, the validity or otherwise of a number of the proposed correlations, and hence the identification of potential basement-cover relationships, is uncertain because of the lack of modern geochronological studies. In this paper we present U-Pb zircon and rutile data and geochemical analyses obtained from meta-igneous and metasedimentary lithologies that crop out in the northeast of the island of Yell in northern Shetland (Fig. 2). The results provide evidence for: 1) the existence of an inlier of Archaean basement that was emplaced tectonically into early Neoproterozoic cover successions, 2) early Neoproterozoic (Tonian) high-grade metamorphism of both basement and cover units, 3) Ordovician and Silurian metamorphism during the Caledonian orogeny. These results provide a firmer basis for regional correlations with other lithotectonic units in the North Atlantic Caledonides.

Regional geological framework of Shetland

The Scottish Caledonides is divided into terranes by major faults (Fig. 1). The western margin of the orogen in mainland Scotland is represented by the Moine Thrust which has traditionally been linked with the Wester Keolka Shear Zone in northwest Shetland (Fig. 1; Andrews 1985; Flinn 1985; Ritchie *et al.* 1987; Flinn 1992; McBride & England 1994; see also Walker *et al*., 2016). To the west is the Laurentian foreland to the Caledonides, the Hebridean Terrane. In mainland Scotland, this is underlain by the Archaean to Palaeoproterozoic Lewisian Gneiss Complex (Friend & Kinny 2001; Love *et al.* 2004; Kinny *et al.* 2005; Wheeler *et al.* 2010). At the supposed equivalent structural position in northwest Shetland, the Uyea and Wilgi Geos orthogneisses of the North Roe area are thought to be of Archaean age also (Flinn *et al.* 1979; Robinson, 1983). Structurally above the Moine Thrust in mainland Scotland is the Northern Highland Terrane which is dominated by the early Neoproterozoic Moine Supergroup (Holdsworth *et al.* 1994; Strachan *et al.* 2002). This was deposited between *c.* 1000 Ma and *c.* 870 Ma near the margin of the *c.* 1.0 Ga Rodinia supercontinent, and affected by Knoydartian orogenic events between 840 Ma and 730 Ma (e.g. Rogers *et al.* 1998; Vance *et al.* 1998; Cutts *et al.* 2010; Cawood *et al.* 2010, 2015). Structurally emplaced inliers of mafic and felsic orthogneisses within the Moine Supergroup have been broadly correlated with the Lewisian Gneiss Complex (Peach *et al.* 1910; Ramsay 1958, 1963; Winchester & Lambert 1970; Moorhouse & Moorhouse 1988; Strachan & Holdsworth 1988; Holdsworth 1989; Friend *et al.* 2008). In northwest Shetland, the psammites of the Sand Voe Group have been correlated on lithological grounds with the Morar Group of the Moine Supergroup (Flinn 1985, 1988). The Sand Voe Group is interleaved with infolds or tectonic slices of hornblende gneisses (Fig. 1) thought to represent inliers of Lewisianoid basement (Flinn *et al.* 1979; Robinson 1983).

In mainland Scotland, the Northern Highland and Grampian terranes are separated by the Great Glen Fault, the northern extension of which is probably the Walls Boundary Fault of Shetland (Flinn 1961, 1977, 1992). The Grampian Terrane in mainland Scotland incorporates the early Neoproterozoic Badenoch Group (possibly correlative with the Moine Supergroup) (Leslie *et al.*, 2013). Correlative lithological units in Shetland may be the metasedimentary gneisses of the Yell Sound and Westing groups (Fig. 1). Both record evidence for amphibolite facies metamorphism at *c.* 930-920 Ma (Cutts *et al.* 2009, 2011) and incorporate strips of mafic and felsic orthogneisses that have been interpreted as inliers of the Lewisian Gneiss Complex (Flinn 1994, 2014). In mainland Scotland and in Shetland, these older metasedimentary successions are overlain by, respectively, the mid-Neoproterozoic to early Cambrian Dalradian Supergroup and the East Mainland Succession (Fig. 1). These were deposited on the margin of

Laurentia during supercontinent breakup and development of the Iapetus Ocean (Anderton 1985; Strachan *et al.* 2002, 2013).

In mainland Scotland, the Highland Boundary Fault is regarded as defining the edge of autochthonous Laurentia. An Ordovician magmatic arc is thought to underlie the Devono-Carboniferous cover of the Midland Valley Terrane (Bluck 1983, 1984, 2001) and its likely northeastern continuation has been identified in the North Sea east of Shetland (Lundmark *et al.* 2014). The collision of this magmatic arc with the margin of Laurentia at *c.* 480-475 Ma was accompanied by obduction of ophiolites (including the Unst ophiolite of northeast Shetland, Fig. 1) and resulted in the Grampian orogenic event (Lambert & McKerrow 1976; Chew *et al.* 2010). This caused widespread metamorphism and deformation of the Moine and Dalradian Supergroups and equivalent units in Shetland (Dewey & Shackleton 1984; Dewey & Ryan 1990; Kinny *et al.* 1999; Oliver *et al.* 2000; Cutts *et al.* 2011; Tanner 2013; Walker *et al.* 2016). The subsequent Silurian collision of Laurentia with Baltica resulted in the *c.* 435-425 Ma Scandian orogenic event. In mainland Scotland, regional deformation and metamorphism of the Moine Supergroup was followed by its northwestward translation along the Moine Thrust (Coward 1990; Dallmeyer *et al.* 2001; Dewey & Strachan 2003). The relative paucity of Silurian mineral ages in Shetland is attributed to a likely location at a high structural level in the regional nappe pile relative to mainland Scotland (Walker *et al.* 2016).

Geology of northeast Yell

The geology of northeast Yell is dominated by the metasedimentary rocks of the Yell Sound Group (Fig. 2). These are mainly gneissic, often migmatitic, psammites with subordinate semipelites and quartzites (Flinn 1994). Minor amounts of calc-silicate rock occur locally but no marble. No sedimentary structures have been preserved and hence the order of succession is unknown. Intrusive bodies of granitic orthogneiss and hornblende-schist (amphibolite) appear to record all the main tectonic and metamorphic events within the host metasedimentary rocks (Flinn 1994).

In northeast Yell, the Yell Sound Group is underlain structurally by a NNW-trending strip of hornblendic and felsic orthogneisses that can be traced farther south onto the island of Hascosay, a total distance of 15 km. Flinn (1988, 1994, 2009) interpreted these orthogneisses (referred to here as the 'Cullivoe orthogneisses') as an inlier of Lewisian basement on lithological grounds. In eastern Yell and on Hascosay (Fig. 1), the orthogneisses structurally overlie psammites, semipelites and marbles of the Westing Group. Flinn (1994) recognised that if the orthogneisses were of Lewisian affinity, this would

require the existence of a tectonic break along the eastern side of Yell which he termed the 'Hascosay Slide', consistent with the often high levels of tectonic strain within all lithological units.

Although tectonic strain within the Cullivoe orthogneisses is often high, it is relatively low on Papil Ness (Fig. 2). Here, banded mafic, intermediate and felsic gneiss are coarsely-layered on all scales by variation in the proportions of hornblende, biotite, quartz and feldspar, enhanced by leucocratic segregations and concordant, pink-orange granitic bands (Fig. 3a and b). Pods up to 10-20 cm wide of hornblendite are wrapped by the gneissic fabric. To the north, on Migga Ness (Fig. 2), the westernmost orthogneisses are two-pyroxene-bearing with isolated boudins of mafic and ultramafic bodies. The eastern part of the outcrop here mainly comprises a 50 x 150 m zone of metagabbro, locally containing a relic garnet-pyroxene metamorphic assemblage. To the south, on the Ness of Cullivoe (Fig. 2), tectonic strain is relatively high and mafic, intermediate and felsic gneisses with subordinate amphibolite mostly carry a strong, regular planar blastomylonitic fabric. Flinn (1994) reported zoned ultramafic pods from Migga Ness and Papil Ness, as well as 7 m wide clinopyroxene- and orthopyroxene-bearing pods from the south end of the Ness of Cullivoe.

Foliation across much of Yell is sub-vertical, although there is a gradual reduction in dip towards the east such that along the coastal strip foliation is generally inclined gently to the west (Fig. 2). Mineral lineations mainly pitch gently north or south irrespective of dip (Flinn 1994). The contacts of the Cullivoe orthogneisses with the Yell Sound and Westing successions are highly strained and associated with blastomylonites. The contact with the Yell Sound Group on Migga Ness is characterised by an oblique-slip sense of shear: mineral lineations trend at ~120 and C-type shear bands indicate a top-to-the-ESE sense of displacement broadly parallel to the lineations. In contrast, the lower contact of the Cullivoe orthogneisses farther south in eastern Yell is associated with sub-horizontal or gently-plunging lineations with no clear sense of shear apparent. There is no discordance in foliation across these contacts that might be consistent with a tectonically modified unconformity between basement and cover, and nor is there any trace within the metasedimentary successions of clasts of material that might have been derived from the orthogneisses.

Sample and zircon characteristics

Samples of orthogneiss and metagabbro were collected from the Cullivoe orthogneisses for U-Pb zircon geochronology and chemistry in order to establish: 1) their protolith age(s) and tectonic affinities, and hence test the hypothesis that these represent a Lewisian-type (i.e. Archaean) basement inlier, and 2) their

subsequent metamorphic history. U-Pb zircon dating was undertaken by either SIMS or by LA-ICPMS. A sample of Yell Sound Group paragneiss was also collected for U-Pb zircon and rutile geochronology by SIMS in order to constrain: 1) its provenance and depositional age by dating detrital zircon grains, and 2) its regional metamorphic history.

SH12-04: Metagabbro [HP 53974 03230]

Sample SH12-04 is from the medium-grained garnet-bearing metagabbro exposed on the eastern margin of Migga Ness (Fig. 2; Fig. 3c). The sample contains the mineral assemblage garnet-orthopyroxene-plagioclase-hornblende-muscovite with accessory ilmenite-rutile-zircon-monazite. Garnet up to 2mm in size is commonly replaced by chlorite. The sample contains a weak west-dipping foliation defined by coarse-grained orthopyroxene. Plagioclase commonly shows extensive sericite alteration and defines a northwest-southeast trending lineation. Zircons are typically anhedral, and range between 50 - 300µm in size. All zircons display cathodoluminescence (CL)-intermediate brightness. Some grains display regular internal boundaries, both narrow and broadly spaced, with thin CL-bright rims that are often discontinuous. Some grains have few or no visible growth zones, many show zones of recrystallisation (Fig. 4a).

SH12-14: Paragneiss (Yell Sound Group) [HP 53736 05217]

The sample is from a 10 m wide shear zone at the boundary between the orthogneisses and the Yell Sound Group to the west (Fig. 2). The mineral assemblage is plagioclase-quartz-biotite-chlorite-muscovite-epidote-chloritoid-garnet, with accessory zircon, ilmenite, rutile and monazite and is characterised by a mylonitic fabric. Interleaved plates of muscovite and chlorite define the foliation on a millimetre scale. Rutile was observed in both random orientations as well as aligned with the foliation. Sample SH12-14 yielded abundant rounded to sub-rounded zircon ranging from 70-200µm in size. Zircon grains comprise two types based on CL-response. Type 1 grains display elongate sub-rounded morphology with cores of intermediate CL brightness surrounded by CL darker rims. Some cores display oscillatory zoning. Type 2 grains are generally ‘soccer ball’ grain shapes, some with weak sector zoning. (Fig. 4b).

SH12-16: Orthogneiss [HP 53780 05241]

The sample is from a narrow (~ 4 m) west-dipping shear zone located in the orthogneiss (SH12-09) (Fig. 2). The mineral assemblage consists of clinopyroxene-plagioclase-quartz-biotite-chlorite-epidote-chloritoid with accessory zircon and monazite. Coarse elongate clinopyroxene and orthopyroxene

replaced by chlorite, biotite and epidote define the strong gneissic foliation. Ductile deformation in the shear zone has resulted in the development of a weak C-type shear band cleavage. Zircon occurs as inclusions in plagioclase and quartz, ranging up to 400 μm in size, and subrounded prismatic to subhedral in shape. Zircon grains comprise two types based on CL-response (Fig. 4c). Type 1 grains display elongate sub-rounded morphology with CL-dark cores often with oscillatory zoning, surrounded by unzoned CL-bright rims. Rims are typically discontinuous and of varying thickness. Type 2 zircons are typically rounded to equant, with zones of recrystallisation and some sector zoning.

SH12-09: Orthogneiss [HP 53982 05217]

Sample SH12-09 is felsic gneiss from the eastern margin of Migga Ness (Fig. 2). The mineral assemblage is quartz-plagioclase-biotite-chlorite-orthopyroxene with accessory zircon, ilmenite and rutile. Gneissic banding is developed on a cm-scale by alternation of felsic layers and streaks with biotite and hornblende-rich bands with some orthopyroxene, and dips moderately to the west. Felsic minerals define a lineation that plunges shallowly to the northwest (Fig. 3d). Zircon grains comprise two types based on CL-response, equivalent to the types observed in sample SH12-16.

11CL-04: Orthogneiss [HP 54921 02599]

The sample is a medium- to coarse-grained felsic gneiss collected near Papil Ness (Fig. 2). Gneissic banding is developed on a cm-scale by alternation of felsic layers and streaks with biotite-rich bands, and dips moderately westwards. The mineral assemblage consists of plagioclase-quartz-biotite with accessory zircon and ilmenite. In thin section, a weak foliation is defined by aligned biotite grains which are commonly replaced by secondary chlorite. Zircons are mostly subhedral and rounded, rarely euhedral. They range from 100 to 300 μm in size and are often made up of a homogeneous dark core in CL, sometimes partially resorbed, surrounded by rims of bright to moderate CL-response (Fig. 5c-h).

11CL-02 Orthogneiss [HP 54054 04479]

The sample is a banded, intermediate orthogneiss collected on the eastern side of the Ness of Cullivoe (Fig. 2). The mineral assemblage consists of feldspar-quartz-hornblende-biotite with accessory ilmenite, zircon and rutile. A weak foliation is defined by aligned hornblende and biotite grains, with the latter occasionally replaced by chlorite**.** Zircons are typically subhedral or rounded and are 100–300 μm in size. In CL, zircons have either a dark core often with oscillatory zoning surrounded by brighter rims, or a moderate to bright homogeneous core with rare thin dark rims (<20 μm) (Fig. 5a-d).

Analytical methods

U-Pb zircon (SIMS)

Zircon from samples SH12-04, SH12-16, SH12-09 and SH12-14 were separated from crushed rock using traditional magnetic and heavy liquid separation techniques. Selected grains chosen to be as representative as possible of the whole population were mounted in epoxy resin with standard zircons (BR266, NBS610 glass, OGC-1 and Temora-2). The grains were imaged using a CL detector fitted to a Phillips XL30 scanning electron microscope (SEM) using a 12kV beam current. CL-images were used to select analysis locations (e.g. Nasdala *et al.*, 2003; Hanchar & Miller, 1993).

Zircon U-Th-Pb isotopic compositions were measured using the Sensitive High Resolution Ion Microprobe (SHRIMP II) instrument at the John de Laeter Centre, Curtin University, Perth, Western Australia. Analytical procedures for the instrument have been described by de Laeter and Kennedy (1998) and Kennedy and de Laeter (1994), and are similar to those described by Compston *et al.* (1984) and Williams (1998). SHRIMP was operated at a mass resolution of 5000, with a primary beam current of 2nA and beam diameter of 20-25µm. Data from the sample were collected successively cyclic field-stepping through the mass range of: $^{196}Zr_2O+$, $^{204}Pb+$, Background, $^{206}Pb+$, $^{207}Pb+$, $^{208}Pb+$, $^{238}U+$, $^{248}ThO+$, $^{254}UO+$. Data were combined after six cycles.

The zircon standards BR266 (Stern and Amelin, 2003) and Temora-2 (Black *et al.*, 2004) were used for $^{206}Pb/^{238}U$ age corrections. Zircon reference material OG1 (Stern et al., 2009) was used to correct for mass fractionation. Common Pb corrections were made using the measured ^{204}Pb in each sample. The common Pb component, being largely surface contaminant, was modelled on the composition of Broken Hill ore Pb. The observed co-variance between Pb+/U+ and UO+/U+ (Compston *et al.*, 1984) obtained from analyses of the standard BR266 (599 ± 0.3 Ma; $^{206}Pb^*/^{238}U$= 0.09059) was used to correct instrumental inter-element discrimination of Pb/U ratios (Stern & Amelin, 2003). Data were processed using SQUID II software and Isoplot/Ex (Ludwig 2003, 2009).

External spot-to-spot errors on zircon U-Pb calibration sessions were <1%, and a minimum error of 1% was applied which reflects the long-term performance of the SHRIMP II facility. Uncertainties assigned to all isotopic ratios and dates for individual analyses in data tables are at the 1σ level. Uncertainties of weighted mean values for pooled analyses in the figures are at the 95 % confidence level. Error ellipses on Concordia diagrams are at the 2σ level. $^{207}Pb/^{206}Pb$ ages are quoted if older than 1.2 Ga, and $^{206}Pb/^{238}U$

ages if younger. Percentage age discordance is defined as the percentage difference between $^{206}Pb/^{238}U$ and $^{207}Pb/^{206}Pb$ ages.

U-Pb rutile (SIMS)

Rutile grains were separated in conjunction with zircon from rock samples by conventional magnetic and heavy liquid separation. Grains were mounted in random orientation in epoxy resin with rutile standard WHQ (Taylor *et al.* 2012). Backscattered electron (BSE) imaging was undertaken in order to choose spot locations. Imaging was conducted on a tungsten-sourced Zeiss EVO SEM at Curtin University, Perth, Western Australia using a 20 kV beam current.

U-Pb isotopic measurements were collected on the SHRIMP II, and analysed using a primary beam current of ~2.5nA , with a beam diameter of approximately 25µm and an impact energy of 10 keV. Corrections for common Pb were made using the measured ^{208}Pb isotope (Hinthorne *et al.* 1979; Compston *et al.*, 1984). An assessment of potential radiogenic ^{208}Pb from Th was made by measuring ThO^+ at mass 264 u.

Pb/U ratios were determined relative to the WHQ (Windmill Hill Quartzite) standard which has a measured age of 2625 Ma, $^{206}Pb^*/^{238}U$ ratio of 0.5025 and U content of 164 ppm (Clark *et al.*, 2000). A fixed slope of 1.12 was used to represent the observed co-variance between Pb^+/UO^+ and UO_2^+/UO^+ for the standard in order to calibrate unknown analyses (Taylor *et al.*, 2012).

U-Pb zircon (LA-ICPMS)

Samples 11CL04 and 11CL02 were crushed using a jaw crusher and disc mill and then sieved to <500 µm. Heavy mineral cuts were separated using a Wilfley table, then zircons were handpicked, mounted in epoxy resin and polished to half height. Grains were imaged using a Phillips XL30CP scanning electron microscope and a CL detector at the University of Portsmouth.

Zircon U–Pb ages were carried by LA-ICPMS at the University of Portsmouth using an Agilent 7500cs (quadrupole) ICP-MS and a New-Wave UP213 (λ=213 nm) solid state Nd:YAG laser, after Jeffries *et al.* (2003). Each analysis consisted of *c.* 30 s background acquisition and 60 s sample acquisition. A 30–40 µm spot was rastered along a 60µm line, with typical laser conditions of a 10 Hz repetition rate and a fluence of *c.* 4 J/cm^2. Ratios were calculated using standard-sample bracketing and an in-house spreadsheet based on LamTool (Košler *et al.*, 2008), measuring GJ-1 (Jackson *et al*., 2004) as the primary

standard and Plešovice and Temora-2 as secondary standards. All uncertainties were propagated in quadrature. GJ-1 yielded a mean $^{206}Pb/^{238}U$ ratio of 0.09758 ± 00251 (MSWD = 0.36, n=58, with 95% confidence limit) and $^{207}Pb/^{206}U$ ratio of 0.06013 ± 00018 (MSWD = 0.3, n=58, with 95% confidence limit), while Plešovice and Temora-2 zircon standards yielded mean $^{206}Pb/^{238}U$ ages of 340.7 ± 3 Ma (2SD; 337.1 ± 0.37 Ma, Sláma *et al.*, 2008) and 419.1 ± 6.3 Ma (95%; 416.78 ± 0.33 Ma, Black *et al.*, 2004) respectively. The amount of ^{204}Pb in these analyses was below the detection limit, and no common Pb correction was undertaken. All zircons of sufficient size were analysed, but only ages from a single growth zone and avoiding irregular features such as cracks and inclusions were used.

Major and trace element chemistry

Samples were split, passed through a jaw-crusher and powdered in a TEMA^{TM} disc mill. Major elements and Sc, Cr, V, Cu, Zn, Ni, Rb, Sr, Y, Zr, Nb, Ba, Pb and Sn were analysed by X-ray fluorescence spectrometry at the University of Portsmouth, against calibrations defined with international certified reference materials (CRMs). Fusion discs were used for the major elements and pressed powder pellets for trace elements. REEs, Hf, Ta, Th and U were analysed by ICP-MS at the University of Portsmouth following fusion dissolutions with Li metaborate (rock:flux ratio 1:3) into 10% HNO_3, also against calibrations defined with international CRMs. Accuracy and precision were monitored with independent CRMs and are both estimated to be better than 1% for major elements and 5% for trace elements.

Results and interpretation: U-Pb geochronology

Zircon

SH12-04: Metagabbro.

Eighteen analyses from this sample plot in a discordant array with upper and lower intercepts at 2687 ± 64 and 977 ± 32 Ma respectively (MSWD = 4.8; Fig. 6a). Taking into account the potential for multi-stage Pb loss, the best estimate of the magmatic zircon age is given by the mean $^{207}Pb/^{206}Pb$ age of those analyses that are within 10% of the upper intercept with Concordia, representing the least isotopically disturbed domains. Additional core analyses together with analyses of rims and recrystallised zones plot further along the array between those ages and the *c*. 946 Ma lower intercept. A group of four analyses consisting of three regularly internally zoned grains and one rim yields a weighted mean $^{207}Pb/^{206}Pb$ age of 2636 ± 150 Ma (2σ, MSWD = 36). The high MSWD, however, suggests that even this sub-group has been

disturbed significantly. Excluding analysis 16.1.1 from the group yields a refined weighted mean $^{207}Pb/^{206}Pb$ age of 2699 ± 48 Ma with acceptable MSWD (2σ, MSWD = 1.2). This value is our best estimate of the protolith age of this sample. At the lower end of the discordance array, three analyses consisting of the recrystallised zones of two zircon and one oscillatory zoned zircon, and that are concordant within error have a weighted mean $^{206}Pb/^{238}U$ age of 944 ± 52 Ma (2σ, MSWD = 2). This value is interpreted as dating metamorphism. The spread in discordant apparent ages is interpreted as variable Pb-loss during this event and subsequent metamorphic event(s).

SH12-16: Orthogneiss

Twenty-two spots were analysed. Analyses targeted the cores and rims of type 1 and type 2 grains. Individual $^{207}Pb/^{206}Pb$ ages range from *c.* 2818 to *c.* 722 Ma. Four analyses were >50% discordant with high common Pb content and large uncertainties, these have been excluded from the plot and age calculations. The remaining data plot in two groups defining a discordia with approximate upper and lower intercepts of 2821 ± 60 Ma and 917 ± 39 Ma respectively (2σ, MSWD = 10.8; Fig. 6c). Given the extent of isotopic disturbance and the lack of near-concordant analyses, this upper intercept age is considered to be the best estimate of the protolith age of this sample. All analyses of rims and recrystallised zones of type 1 grains, one type 1 grain, and all type 2 grains define a younger population with $^{206}Pb/^{238}U$ ages ranging from *c*. 1006-835 Ma. Analyses that are <10% discordant at the lower end of the discordance array yielded a weighted mean $^{206}Pb/^{238}U$ age of 931 ± 29 Ma (2σ, MSWD = 7.1; Fig. 6d). Given that these analyses have distinctly low Th/U with respect to typical magmatically crystallised zircon (e.g. Hancher and Miller, 2003; Corfu *et al.* 2003) and that they are from unzoned rims of predominantly CL-bright responses or unzoned recrystallised grains, this age is considered a best estimate of the time of new zircon growth during metamorphism. The high MSWD of this grouping, however, together with attendant discordant analyses indicates that additional, later isotopic disturbance has occurred.

SH12-09: Orthogneiss

Seventeen analyses were made of zircons from this sample. Both cores and rims of grains were analysed. All analyses were between 14 and 39 % discordant (Fig. 6b). Although the plotted data points do not define a meaningful discordance line, the majority of analyses have apparent $^{207}Pb/^{206}Pb$ ages ranging from *c.* 2674 Ma to *c.* 2250 Ma, consistent with a late Archaean magmatic crystallization age and later

disturbance. Two analyses record distinctly older Archaean $^{207}Pb/^{206}Pb$ ages of *c.* 3079 Ma and *c.* 3030 Ma, these may represent pre-magmatic inherited zircon.

SH12-14: Paragneiss

Twenty-three analyses were obtained from twenty-one zircons. Analyses targeted the cores and rims of type 1 and type 2 grains. Cores of type 1 grains are interpreted to be detrital based on the presence of concentric zoning and typical magmatic Th/U ratios. Rims of type 1 zircon and grains of type 2 are interpreted to be metamorphic based on their morphology. The majority of analyses plot close to Concordia (Fig. 6e). Three analyses with large uncertainties have been excluded from the plot, analysis with >10% discordant have been excluded from age calculations. The inferred detrital grains have apparent $^{207}Pb/^{206}Pb$ ages ranging from *c.* 3113 to *c.* 1019 Ma with Th/U ratios between 0.08-0.71 (Fig.6e-f). Analyses of type 1 rims and type 2 grains yielded a weighted mean $^{206}Pb/^{238}U$ age of 906 ± 33 Ma (2σ, MSWD = 13). The high MSWD indicates a significant spread in ages, and probably reflects the additional Caledonian disturbance of the original metamorphic grains. Three analyses with $^{206}Pb/^{238}U$ ages ranging from 859 to 865 Ma with lower Th/U ratios (0.2-0.3; Fig. 6f), are excluded and are interpreted to reflect minor loss of radiogenic Pb, resulting in partially reset grains. The remaining analyses form a single population with lower Th/U ratios (<0.03) than the inferred detrital grains, with a weighted mean $^{206}Pb/^{238}U$ age of 941 ± 16 Ma (2σ, MSWD = 1.4; Fig. 6f). This age is considered to be the best estimate of the timing of new zircon growth during metamorphism.

11CL-04

Thirty-seven spots were analysed, of which fourteen plot in a broad discordant array with upper and lower intercepts crossing Concordia at 2702 ± 71 Ma and 1229 ± 100 Ma respectively (MSWD = 8.9; Fig. 7c). Eight analyses of zircon cores that are either homogeneous or show oscillatory zoning, plot close to Concordia (<5.3% discordant) at the upper end of the array. These analyses range in $^{207}Pb/^{206}Pb$ age from 2814 to 2630 Ma and are interpreted as magmatic zircons that have experienced some early isotopic disturbance to produce the observed spread in apparent ages. Additional core analyses together with analyses of bright and intermediate rims plot further along the array between those ages and the *c.* 1229 Ma lower intercept. The analyses defining the array plot along most of its length, and are interpreted to record variable resetting by the regional Neoproterozoic high-temperature metamorphic event. However, no concordant analyses of that age were obtained. Instead, three analyses of dark zircon rims with low

Th/U define a younger population with a weighted mean $^{206}Pb/^{238}U$ age of 482 ± 30 Ma (2σ, MSWD = 2.5; Fig. 7d). This distinctly younger age records an episode of further metamorphism that resulted in the growth of new zircon rims, some grains showing distinct morphological overgrowths (grain 38, Fig. 5f).

11CL-02

Nineteen analyses from this sample plot in a discordant array with upper and lower intercepts at 2856 ± 44 Ma and 946 ± 23 Ma respectively (MSWD = 6.7; Fig. 7a). The analysed magmatic cores generally have a higher U content (78–341 ppm) than other parts of the grains, accounting for their darker appearance in CL. Those core analyses which are <10% discordant record $^{207}Pb/^{206}Pb$ ages ranging between 2983 and 2747 Ma. A distinct younger zircon population consisting of five cores of rounded zircons and four CL-intermediate rims, with the have the low Th/U signature that is typical of metamorphic zircon, record a weighted mean $^{206}Pb/^{238}U$ age of 940 ± 14 Ma (2σ, MSWD = 1.4; Fig. 7b). This younger concordant population is interpreted to again represent the high-temperature metamorphic event which also affected some of the magmatic Archaean zircons. Unlike sample 11-CL04, a younger Ordovician metamorphic age has not been identified in this sample but could be represented in narrow dark rims observed on some zircons that were too small to be analysed.

Rutile

SH12-14

Rutile from sample SH12-14 showed no signs of alteration nor systematic zonation in back-scattered electron images, therefore only one analysis per grain was made. Thirty-five grains were analysed. The data define a close population (Fig. 8) with apparent $^{206}Pb/^{238}U$ ages ranging from *c.* 484 to *c.* 345 Ma. Nine analyses with large uncertainties have been excluded from the plot and age calculations. Twenty-six analyses were combined to yield a weighted mean $^{206}Pb/^{238}U$ age of 428 ± 16 Ma (2σ, MSWD 0.62; Fig. 8). This age is interpreted to represent post-metamorphic cooling.

Results and interpretation: major and trace element chemistry

A suite of ten samples of the Cullivoe gneisses was collected for the purposes of whole-rock chemistry. Two of these (11CL-02 and 11CL-04) provided zircons for dating, described above. Representative elemental data are presented in Table 5. Silica ranges from 45.22 to 51.21 wt % in the mafic gneisses,

associated with the following oxide ranges: TiO_2 from 1.32 to 3.00 wt %, Al_2O_3 from 12.51 to 20.14 wt %, Fe_2O_3 (T) from 9.08 to 23.65 wt %, MnO from 0.12 to 0.32 wt %, MgO from 2.46 to 5.27 wt %, CaO from 8.21 to 10.78 wt %, Na_2O from 1.90 to 4.54 wt %, K_2O from 0.17 to 0.29 wt %, P_2O_5 from 0.09 to 0.18 wt %. For the felsic gneisses the following ranges apply: SiO_2 from 63.66 to 70.27 wt %, TiO_2 from 0.26 to 0.88 wt %, Al_2O_3 from 14.28 to 17.05 wt %, Fe_2O_3 (T) from 3.97 to 7.58 wt %, MnO from 0.02 to 0.09 wt %, MgO from 0.64 to 3.35 wt %, CaO from 2.64 to 4.43 wt %, Na_2O from 2.24 to 4.69 wt %, K_2O from 0.61 to 2.72 wt %, P_2O_5 from 0.05 to 0.12 wt %. Harker diagrams (Fig. 9) display decreasing Fe_2O_3, MgO, TiO_2 and P_2O_5 amongst the mafic gneisses, with increasing Al_2O_3, CaO and Na_2O. K_2O is uniformly low. For the felsic gneisses, there are strongly decreasing trends with SiO_2 for MgO, Fe_2O_3, TiO_2, K_2O and P_2O_5, and broadly increasing for Na_2O and Al_2O_3. On a plutonic total alkalis versus silica plot (Fig. 10) the data are bimodal, with mafic gneisses falling in the gabbro field and the felsic gneisses in the granodiorite-granite fields. However, on a normative Ab-An-Or diagram (Fig. 11a, Barker, 1979), the felsic gneisses plot as tonalities and granodiorites, according rather better with their mineralogy which often lacks abundant K-feldspar. On an AFM diagram (Fig. 11b) the mafic gneisses fall in the tholeiitic field while the felsic gneisses plot as calc-alkaline.

Trace element abundances are summarised with selected Harker-style diagrams in Fig. 9. Alkali and alkaline earth metals are higher in the felsic rocks (e.g. Rb a few tens of ppm, Sr and Ba several hundreds of ppm). Rb is closely correlated with K_2O, with high K/Rb ratios, consistent with granulite facies metamorphism of the protoliths. Of the high field-strength elements, Zr is more abundant in the felsic rocks (hundreds of ppm vs. single-figure ppm), but Y is considerably lower (single-figure ppm but cf. a few tens in the mafic rocks). Th (not shown) is very low (< 1 ppm) in relation to Archaean crustal averages of 5.7 ppm and 3.8 ppm (upper crust and bulk crust values: Taylor and McLennan, 1985), with the exception of sample 11CL-03 at a more normal 4.7 ppm, again possibly indicative of granulite-facies metamorphism. Predictably, transition metals are higher in the mafic rocks (Sc, Cr and Ni a few tens of ppm; V, Cu and Zn (not shown) are a few hundred ppm) than the felsic ones and generally fall with silica abundance.

In rocks such as these with a protracted metamorphic history, petrogenetic constraints are best derived from relatively immobile trace elements such as the rare earth elements (REEs), whose abundances are displayed as chondrite-normalised plots in Fig. 12. Even so, given the presence of garnet in the mafic rocks, these should be treated with some caution. The majority of the mafic gneisses show flat heavy

REEs at 20-40 times chondrites, insignificant Eu anomalies and mild light-REE depletion. One sample (08MN-02) has a significant positive Eu anomaly and mild light-REE enrichment. On the other hand, the felsic gneisses show low heavy REE, large positive Eu anomalies in the more silicic examples and strong light-REE enrichment. These features are sufficiently distinct to preclude a direct genetic relationship between the gneiss types. The mafic gneisses are likely to have been derived as tholeiitic magmas from a depleted mantle source, but must have undergone significant fractionation (olivine ± pyroxene) in order to reduce Cr and Ni abundances. La and Eu-rich sample 08MN-02 has ca. 20 wt% Al_2O_3 and the highest Sr of the mafic gneisses sampled (264 ppm): it may therefore have been enriched in cumulus plagioclase. The range of REE patterns generally falling with increasing SiO_2, plus the large positive Eu anomalies and concave-upward heavy-REE patterns in the more silicic rocks, strongly suggest amphibole involvement either as a residual phase during melting or during fractional crystallisation.

Discussion

Ages of the igneous protoliths of the Cullivoe orthogneisses

U-Th-Pb SIMS analyses of zircon from samples SH12-04 and SH12-16 have yielded data that provide estimates of original igneous protolith ages. These estimates are from the upper intercepts of the discordant array from sample SH12-16 (2821 ± 60 Ma) and discrete, near concordant population of zircon core and recrystallised growth domains from sample SH12-04 (2699 ± 48 Ma). U-Pb LA-ICPMS analyses of zircon from samples 11CL-04 and 11CL-02 have also yielded discordant arrays, with upper intercepts of 2702 ± 71 Ma and 2856 ± 44 Ma, respectively. These upper intercept ages are similarly interpreted as providing estimates of protolith ages. The orthogneiss protolith ages indicate Neoarchean crystallisation ages which range between *c.* 2850 Ma to *c.* 2700 Ma. These ages provide the first constraints on the age of emplacement of the basement gneisses in this area, and are broadly in agreement with K-Ar ages of *c.* 2873 Ma (Flinn *et al.*, 1979) and U-Pb zircon ages of *c.* 2870-2730 Ma (Davis, 2012; Kinny & Strachan unpublished data) obtained from gneisses of the Uyea Group, North Roe, which lie west of the Walls Boundary Fault on mainland Shetland (Fig.1).

Provenance and age of the Yell Sound Group

Sample SH12-14 yielded insufficient detrital zircons for statistical analysis. However, concordant analyses of interpreted detrital grains of igneous origin have ages ranging between 3113-1019 Ma. In combination with the interpreted metamorphic zircon ages of *c.* 941 Ma (see below), the data indicate

deposition of the sedimentary protolith between *c.* 1019 Ma and *c.* 941 Ma. The ages of the youngest detrital grains in SH12-14 are broadly consistent with the U-Pb zircon age of the main detrital peak reported by Cutts *et al.* (2009) from metasedimentary sample SH11 of the Westing Group on the west coast of Unst (Fig. 1).

Neoproterozoic metamorphism

Three samples have yielded U-Pb SIMS data that provide estimates for the age of high-temperature metamorphism in the Neoproterozoic. These data are from concordant populations of zircon rims and metamorphic growth domains characterised by distinctly low Th/U ratios from samples SH12-04, SH12-14 and SH12-16. These returned weighted mean $^{206}Pb/^{238}U$ ages of 944 ± 52 Ma, 941 ± 16 Ma and 931 ± 29 Ma, respectively. This Neoproterozoic (Tonian) metamorphic event represents the principal time of isotopic disturbance of the protolith zircons as well as a time of growth of new zircon. These findings are consistent with the U-Pb LA-ICPMS data obtained from samples 11CL-04 and 11CL-02, the discordant arrays recording lower intercept ages of 984 ±120 Ma and 933 ± 51 Ma respectively, and a distinct population of low Th/U rims and rounded grains within 11CL-02 yielding weighted mean $^{206}Pb/^{238}U$ age of 940 ± 14 Ma. In summary, the data indicate that the Cullivoe orthogneisses and the Yell Sound Group both record a high-temperature metamorphic event at *c.* 940-930 Ma, similar to the *c.* 938-925 Ma age deduced by Cutts *et al.* (2009) for early Neoproterozoic metamorphism in the nearby Westings Group.

Caledonian metamorphism

The age of 482 ± 30 Ma derived from three concordant analyses from sample 11CL-04 is most easily interpreted as corresponding to the time of high-grade metamorphism during the Ordovician Grampian orogenic event (Oliver *et al.* 2000; Chew *et al.* 2010; Cutts *et al.* 2011; Crowley & Strachan, 2015). The U-Pb rutile age of 428 ± 16 Ma obtained from sample SH12-14 is interpreted as representing the timing of the youngest metamorphic event the Yell Sound Group experienced during the Scandian orogenic event in the Silurian. As the mineral assemblage in the dated sample is mylonitic, consisting of low-moderate temperature metamorphic minerals muscovite, chlorite and epidote, this might suggest that Silurian metamorphism was associated with shearing at greenschist facies conditions. However, because rutile grains locally overprint the mylonite fabric it is possible that this foliation formed during an older event.

Implications for regional correlations

The new data reported here confirm the hypothesis of Flinn (1994, 2009) that the Cullivoe orthogneisses likely correlate in a broad way with the Lewisian Gneiss Complex of the Hebridean Terrane in mainland Scotland and the Hebrides. The protolith ages of the Cullivoe orthogneisses are similar to those recorded by many of the older components of the Lewisian Gneiss Complex (e.g. Kinny *et al.* 2005; Wheeler *et al.* 2010), representing a period of significant Neoarchaean crustal growth in the North Atlantic Craton (e.g. Garde *et al.*, 2000; Nutman *et al.*, 2010; Tappe *et al.*, 2011; Dyck *et al.*, 2015). The geochemical characteristics of the felsic components of the Cullivoe orthogneisses are typical of tonalite-trondhjemite-granodiorite (TTG) suite rocks of the kind that dominate the Lewisian Gneiss Complex (Rollinson & Fowler 1987; Fowler & Plant 1987) and Archaean cratons globally (Moyen & Martin 2012). There is sufficient spread amongst the less-disturbed Archaean zircons (especially in sample 11CL-04) to suggest that isotopic disturbance had occurred prior to the 940-930 Ma event. We have no precise constraints on the timing of this early isotopic disturbance, but suggest that it most likely occurred during the *c.* 1.8-1.7 Ga Laxfordian event which was a period of major reworking at high metamorphic grade of significant tracts of the Lewisian Gneiss Complex (Kinny et al. 2005; Wheeler et al. 2010 and references therein). The inferred detrital zircon data from SH12-14, in combination with the metamorphic zircon ages, indicate that deposition of the Yell Sound Group occurred between *c.* 1019- 940 Ma, during or shortly after the assembly of Rodinia at *c.* 1.2-1.0 Ga (Cawood *et al.*, 2007). Broad correlation with the Torridon Group of the Hebridean Terrane and the Morar Group of the Moine Supergroup would be feasible if deposition occurred after *c.* 990-980 Ma. The Yell Sound Group is not lithologically similar to either succession, but could have been deposited in a contemporaneous but entirely separate and distal basin. Correlation of the Yell Sound Group with the Glenfinnan Group was proposed on lithological grounds by Flinn (1988) but this is now ruled out as the latter is thought to have been deposited after *c.* 920 Ma (Cutts *et al.* 2011; Cawood *et al.* 2015).

U-Pb zircon evidence for a high-temperature metamorphic event within the Cullivoe orthogneisses and the Yell Sound Group at *c.* 940 Ma is consistent with emerging data sets from peri-Laurentian terranes around the North Atlantic region. Recent geochronological investigations synthesised by Cawood *et al.* (2010) have revealed two major cycles of sedimentation and orogenesis along the northern Laurentian margin in the North Atlantic region between 1030-710 Ma (see also Kirkland *et al.*, 2011; Malone *et al.* 2014). These events are recorded in regions currently exposed in Scotland, Shetland, East Greenland, Svalbard,

Pearya and Norway and are currently interpreted in the context of the development of an exterior, accretionary 'Valhalla' orogen along the margin of Rodinia (Cawood *et al.*, 2010). An early 'Renlandian' phase of deformation, metamorphism and granite intrusions occurred between 980-920 Ma. It is this event that resulted in the high-temperature reworking of the Cullivoe orthogneisses and early metamorphism of the Yell Sound Group as well as the Westing Group (Cutts *et al.*, 2009).

Thermal rejuvenation during the Caledonian orogeny is represented by the U-Pb zircon age of 482 ± 30 Ma from the Cullivoe orthogneisses and the U-Pb rutile age of 428 ± 16 Ma from the Yell Sound Group. Both ages are consistent with the *c.* 467 to *c.* 451 Ma monazite ages from northeasten Shetland reported by Cutts *et al*. (2011) and the currently understood tectonic framework for the Caledonian orogeny, involving Ordovician arc-continent collision and final continental amalgamation in the Silurian (e.g. Dewey & Ryan 1990; Dallmeyer et al. 2001; Chew et al. 2010). Cutts *et al.* (2011) did not find isotopic evidence of the *c.* 430 Ma Silurian metamorphic event recorded in the YSG. However, this sample was obtained from a shear zone, and the 428 ± 16 Ma rutile age obtained from sample SH12-14 could reflect reactivation of the shear zone during the Scandian event. It is also possibly attributed the lower closure temperature of rutile compared to monazite, ~ 600°C (Cherniak, 2000), and could represent cooling from the peak temperatures (*c.* 650°C) defined by Cutts *et al.* (2011) for meta-igneous lithologies on Yell and Unst. This age is reflected in *c*. 420 Ma K-Ar and $^{40}Ar/^{39}Ar$ mineral ages from northeast Unst (Flinn & Oglethorpe, 2005).

Structural setting of the Cullivoe orthogneisses

The isotopic data reported here have established that the Cullivoe orthogneisses constitute an inlier of Neoarchaean basement; outstanding issues relate to how and when it was interleaved tectonically with the Yell Sound and Westing successions. Consideration of these issues is made problematic by the generally high tectonic strains within, and along the margins of, the inlier. Because the metasedimentary successions west and east of the inlier differ lithologically (Flinn 1994), this means that the inlier cannot simply occupy the core of a major isoclinal fold. Either its eastern or western boundary must represent a significant tectonic break, and it is therefore possible that the other boundary could be a tectonically-modified unconformity with either the Yell Sound Group or the Westing Group. However, the regionally gently-plunging mineral lineations are not commonly associated with kinematic indicators, suggesting a strain regime close to overall bulk pure shear. The deformation event that produced these structures is thus unlikely to have been responsible for the primary interleaving of basement and cover, but instead

reworked a pre-existing basement-cover relationship. We therefore suggest that Flinn's (1994) 'Hascosay Slide' is an early tectonic break, most probably a thrust, located along either the western or eastern edge of the Cullivoe orthogneisses, but entirely cryptic as a result of the intensity of Caledonian reworking.

Conclusions

(1) The geochemical characteristics of the felsic components of the Cullivoe orthogneisses are typical TTG suite rocks. The igneous protoliths of the orthogneisses and metagabbro of the Cullivoe inlier crystallised at *c.* 2856-2699 Ma. Their evolution is broadly coeval with development of the protoliths of the Lewisian Gneiss Complex of mainland Scotland and the Outer Hebrides, and a major period of Neoarchaean crustal growth in the North Atlantic Craton.

(2) Deposition of the sedimentary precursors of the Yell Sound Group occurred between *c.* 1019 Ma (the age of the youngest detrital zircon grain) and *c.* 941 Ma (the age of the oldest metamorphic event to affect these rocks). If sedimentation occurred <1000 Ma, the Yell Sound Group might be coeval with the Torridon Group and Morar Group of mainland Scotland, but correlation with the younger (<920 Ma) parts of the Moine Supergroup (Glenfinnan and Loch Eil groups) is ruled out.

(3) Both the Cullivoe inlier and the Yell Sound Group were metamorphosed at *c.* 944-931 Ma, with the former containing granulite facies mineral assemblages inferred to be of this age. Similar-aged Tonian metamorphic events have been recorded in various Laurentian sedimentary successions in the North Atlantic region and attributed to development of an accretionary Valhalla orogeny along the margin of Rodinia (Cawood *et al.* 2010).

(4) Thermal rejuvenation during the Ordovician (482 ± 30 Ma) and the Silurian (428 ± 16 Ma) resulted from successive phases of the Caledonian orogeny during closure of the Iapetus Ocean.

(5) The mechanism by which the Cullivoe inlier was emplaced into its current structural setting in relation to the adjacent Yell Sound and Westing groups is uncertain. Either its western or eastern boundary must represent a major tectonic break, most likely an early ductile thrust of Tonian or Ordovician age. However, this structure is now entirely cryptic as a result of intense ductile reworking during the Caledonian orogeny.

Acknowledgments: Funding for fieldwork and analytical work were provided through Australian Research Council (ARC) project DE120103067 to C. Clark. Zircon and rutile U-Pb analyses were carried

549 out using the SHRIMP-II Ion Microprobe at the John de Laeter Centre, Perth, managed by Allen Kennedy
550 on behalf of a consortium consisting of Curtin University, the Geological Survey of Western Australia,
551 and the University of Western Australia with the support of the Australian Research Council. The
552 geochemistry and other zircon analyses were carried out at the University of Portsmouth. We also
553 acknowledge the facilities, scientific and technical assistance of the Centre for Microscopy,
554 Characterisation and Analysis. We thank Craig Storey for discussions in the field.

555 **Supplementary data:** Supplementary data associated with this article include LA-ICPMS U-Th-Pb data
556 for zircon standards (Table 1.), ion microprobe U-Th-Pb age data for zircon from samples SH12-004,
557 SH12-009, SH12-014 and SH12-016 (Table 2.), LA-ICPMS U-Th-Pb age data for zircon from samples
558 IICL-02 and IICL-04 (Table 3.), ion microprobe U-Th-Pb age data for rutile from samples SH12-014
559 (Table 4.) and major and trace element results for selected samples (Table 5.).

560 ## References

561 Anderton, R. 1985. Sedimentation and tectonics in the Scottish Dalradian. *Scottish Journal of Geology*,
562 **21**(4), 407-436.

563 Andrews, I. J. 1985. The deep structure of the Moine Thrust, southwest of Shetland. *Scottish Journal of*
564 *Geology*, **21**(2), 213-217.

565 Barker, F. 1979. Trondhjemite:definition, environment and hypotheses of origin. *In:* Barker, F. (ed)
566 *Trondhjemites, Dacites and Related Rocks*, Elsevier, Amsterdam, 1-12.

567 Black, L.P., Kamo, S.L., Allen, C.M., Davis, D.W., Aleinikoff, J.N.,Valley, J.W., Mundil, R., Campbell,
568 I.H., Korsch, R.J., Williams, I.S. & Foudoulis, C. 2004. Improved $^{206}Pb/^{238}U$ microprobe
569 geochronology by the monitoring of a trace-element-related matrix effect; SHRIMP, ID-TIMS,
570 ELA-ICP-MS and oxygen isotope documentation for a series of zircon standards. *Chemical*
571 *Geology*, **205**, 115–140.

572 Bluck, B. J. 1983. Role of the Midland Valley of Scotland in the Caledonian orogeny. *Transactions of the*
573 *Royal Society of Edinburgh: Earth Sciences*, **74**(03), 119-136.

574 Bluck, B. J. 1984. Pre-Carboniferous history of the Midland Valley of Scotland. T*ransactions of the Royal*
575 *Society of Edinburgh: Earth Sciences,* **75**(02), 275-295.

576 Bluck, B.J. 2001. Caledonian and related events in Scotland: *Transactions of the Royal Society of*
577 *Edinburgh Earth Sciences*, **91**, 375-404.

578 Cawood, P.A., Menchin, A.A., Strachan, R.A., Prave, A.R. & Krabbendam, M. 2007. Sedimentary basin
579 and detrital zircon record along East Laurentia and Baltica during assembly and breakup of
580 Rodinia. *Journal of the Geological Society, London*, **164**, 257-275.

581 Cawood, P. A., Strachan, R., Cutts, K., Kinny, P. D., Hand, M., & Pisarevsky, S. 2010. Neoproterozoic
582 orogeny along the margin of Rodinia: Valhalla orogen, North Atlantic. *Geology*, **38**(2), 99-102.

583 Cawood, P. A., Strachan, R. A., Merle, R. E., Millar, I. L., Loewy, S. L., Dalziel, I. W. D., Connelly, J. N.
584 2015. Neoproterozoic to early Paleozoic extensional and compressional history of East
585 Laurentian margin sequences: The Moine Supergroup, Scottish Caledonides. *Geological Society*
586 *of America Bulletin*, **127**, 349-371

587 Cherniak, D.J. 2000. Pb diffusion in rutile. *Contributions to Mineralogy and Petrology*, **139**, 198-207.

588 Chew, D. M., Daly, J. S., Magna, T., Page, L. M., Kirkland, C. L., Whitehouse, M. J., & Lam, R. 2010.
589 Timing of ophiolite obduction in the Grampian orogen. *Geological Society of America Bulletin*,
590 **122**(11-12), 1787-1799.

591 Clark, D.J., Hensen, B.J. & Kinny, P.D. 2000. Geochronological constraints for a two-stage history of the
592 Albany-Fraser Orogen, Western Australia. *Precambrian Research*, **102**(3-4), 155-183

593 Compston, W., Williams, I.S. & Meyer, C. 1984. U-Pb Geochronology of Zircons from Lunar Breccia
594 73217 Using a Sensitive High Mass-Resolution Ion Microprobe. *Journal of Geophysical Research*,
595 ***89***, (suppl.), B525-B534.

596 Coward, M. P. 1990. The Precambrian, Caledonian and Variscan framework to NW Europe. *Geological*
597 *Society, London, Special Publications*, **55**(1), 1-34.

598 Crowley, Q. G., & Strachan, R. A. 2015. U–Pb zircon constraints on obduction initiation of the Unst
599 Ophiolite: an oceanic core complex in the Scottish Caledonides? *Journal of the Geological Society,*
600 *London*, **172**(3), 279-282.

601 Cutts, K. A., Hand, M., Kelsey, D. E., Wade, B., Strachan, R. A., Clark, C., & Netting, A. 2009. Evidence
602 for 930 Ma metamorphism in the Shetland Islands, Scottish Caledonides: implications for

603 Neoproterozoic tectonics in the Laurentia–Baltica sector of Rodinia. *Journal of the Geological*
604 *Society, London* **166**(6), 1033-1047.

605 Cutts, K. A Kinny, P. D., Strachan, R. A., Hand, M., Kelsey, D. E., Emery, M., Leslie, A. G. 2010. Three
606 metamorphic events recorded in a single garnet: Integrated phase modelling, in situ LA-ICPMS
607 and SIMS geochronology from the Moine Supergroup, NW Scotland. *Journal of Metamorphic*
608 *Geology*, **28**(3), 249–267.

609 Cutts, K. A., Hand, M., Kelsey, D. E., & Strachan, R. A. 2011. P–T constraints and timing of Barrovian
610 metamorphism in the Shetland Islands, Scottish Caledonides: implications for the structural setting
611 of the Unst ophiolite. *Journal of the Geological Society, London*, **168**(6), 1265-1284.

612 Dallmeyer, R. D., Strachan, R. A., Rogers, G., Watt, G. R., & Friend, C. R. L. 2001. Dating deformation
613 and cooling in the Caledonian thrust nappes of north Sutherland, Scotland: insights from $^{40}Ar/^{39}Ar$
614 and Rb–Sr chronology. *Journal of the Geological Society, London* ,**158**(3), 501-512.

615 Davis, S.P. 2012. Geological relationships of the basement gneisses of North Roe, Shetland. Unpublished
616 Honours thesis, Curtin University of Technology, Perth, Australia.

617 De Laeter, J. R., & Kennedy, A. K. 1998. A double focusing mass spectrometer for geochronology.
618 *International Journal of Mass Spectrometry*, **178**(1), 43-50.

619 Dewey, J.F. & Shackleton, R.M., 1984. A model for the evolution of the Grampian Tract in the early
620 Caledonides and Appalachians. *Nature*, **312**, 115-121.

621 Dewey, J.F. & Ryan, P.D., 1990. The Ordovician evolution of the South Mayo Trough, western Ireland:
622 *Tectonics*, **9**, 887-901.

623 Dewey, J. F., & Strachan, R. A. 2003. Changing Silurian–Devonian relative plate motion in the
624 Caledonides: sinistral transpression to sinistral transtension. *Journal of the Geological Society,*
625 *London*, **160**(2), 219-229.

626 Dyck, B., Reno, B. L., & Kokfelt, T. F. 2015. The Majorqaq Belt: A record of Neoarchaean orogenesis
627 during final assembly of the North Atlantic Craton, southern West Greenland. *Lithos*, **220**, 253-271.

628 Flinn, D. 1961. Continuation of the Great Glen Fault beyond the Moray Firth. *Nature*, **191,** 589-591.

629 Flinn, D. 1977. Transcurrent faults and associated cataclasis in Shetland. *Journal of the Geological*
630 *Society*, **133**(3), 231-247.

631 Flinn, D. 1985. The Caledonides of Shetland. In: Gee, D.G and Sturton, B.A.. (eds) *The Caledonide*
632 *Orogen - Scandinavia and Related Areas*. Wiley & Sons, New York, 1159-1172.

633 Flinn, D. 1988. The Moine rocks of Shetland. In: Winchester, J.A. (ed.) *Later Proterozoic Stratigraphy of*
634 *the Northern Atlantic Regions*. Blackie, Glasgow, 74-85.

635 Flinn, D. 1992. The history of the Walls Boundary fault, Shetland: the northward continuation of the
636 Great Glen fault from Scotland. *Journal of the Geological Society, London*, **149**(5), 721-726.

637 Flinn, D. & Oglethorpe, R.J.D. 2005. A history of the Shetland Ophiolite Complex. *Scottish Journal of*
638 *Geology*, **41**, 141-148.

639 Flinn, D. 1994. Geology of Yell and some neighbouring islands in Shetland. Memoir of the Brithish
640 Geological Survey, Sheet 130 (Scotland).

641 Flinn, D. 2009. Lewisian and Moine of Shetland. *In*: Mendum, J.R., Barber, A.J., Butler, R.W.H., Flinn,
642 D., Goodenough, K.M., Krabbendam, M., Park, R.G. & Stewart, A.D., *Lewisian, Torridonian and*
643 *Moine Rocks of Scotland*, Geological Conservation Review Series, No. 34, Joint Nature
644 Conservation Committee, Peterborough, 623-650.

645 Flinn, D. 2014. *Geology of Unst and Fetlar in Shetland: memoir for 1: 50 000 geological sheet 131*
646 *(Scotland) Unst and Fetlar* (Vol. 131). British Geological Survey.

647 Flinn, D., May, F., Roberts, J.L. & Treagus, J.E. 1972. A revision of the stratigraphic succession of the
648 East Mainland in Shetland. *Scottish Journal of Geology*, **8**, 335-343.

649 Flinn, D., Frank, P.L., Brook, M. & Pringle, I.R. 1979. Basement-cover relations in Shetland. *In*: Harris,
650 A.L., Holland, C.H. & Leake, B.E. (eds) *The Caledonides of the British Isles - Reviewed*.
651 Geological Society, London, Special Publications, **8,** 109-115.

652 Fowler, M.B. & Plant, J.A. 1987. Rare earth element geochemistry of Lewisian grey gneisses from
653 Gruinard Bay. *Scottish Journal of Geology*, **23**, 193-202.

654 Friend, C., & Kinny, P. 2001. A reappraisal of the Lewisian Gneiss Complex: geochronological evidence
655 for its tectonic assembly from disparate terranes in the Proterozoic. *Contributions to Mineralogy*
656 *and Petrology*, **142**(2), 198-218.

Friend, C. R. L., Strachan, R. A., & Kinny, P. D. 2008. U–Pb zircon dating of basement inliers within the Moine Supergroup, Scottish Caledonides: implications of Archaean protolith ages. *Journal of the Geological Society, London,* **165**(4), 807-815.

Garde, A. A., Friend, C. R., Nutman, A. P., & Marker, M. 2000. Rapid maturation and stabilisation of middle Archaean continental crust: the Akia terrane, southern West Greenland. *Bulletin of the Geological Society of Denmark,* **47**, 1-27.

Hanchar, J.M. & Miller, C.F. 1993. Zircon zonation patterns as revealed by cathodoluminescence and backscattered electron images: Implications for interpretation of complex crustal histories. *Chemical Geology,* **110**, 1-13.

Hinthorne, J.R., Andersen, C.A., Conrad, R.L., & Lovering, J.F. 1979.Single-grain $^{207}Pb/^{206}Pb$ and U/Pb age determinations with a 10 μm spatial resolution using the ion microprobe mass analyzer (IMMA): *Chemical Geology*, **25**, 271–303.

Holdsworth, R.E. 1989. The geology and structural evolution of a Caledonian fold and ductile thrust zone, Kyle of Tongue region, Sutherland, northern Scotland. *Journal of the Geological Society, London,* **146,** 809-823.

Holdsworth, R. E., Strachan, R. A., & Harris, A. L. 1994. Precambrian rocks in northern Scotland east of the Moine Thrust: the Moine Supergroup. *In:* Gibbons, W. & Harris, A.L. (eds) A Revised Correlation of Precambrian Rocks in the British Isles. *Geological Society, London, Special Reports*, **22**, 23-32.

Jackson, S.E., N.J. Pearson, W.L. Griffin, E.A. Belousova. 2004. The application of laser ablation-inductively coupled plasma-mass spectrometry to in situ U/Pb zircon geochronology. *Chemical Geology*, 211, 47–69.

Jeffries, T.E., Fernandez-Suarez, J., Corfu, F. & Alonso, G.G. 2003. Advances in U–Pb geochronology using a frequency quintupled Nd:YAG based laser ablation system (λ = 213 nm) and quadrupole based ICP-MS. *Journal of Analytical Atomic Spectrometry*, **18**, 847-855.

Kennedy A.K. and de Laeter J.R. 1994. The performance characteristics of the WA SHRIMP II ion microprobe. *In*: 8th International Conference on Geochronology, Cosmochronology and Isotope Geology, Berkeley. *USGS Circular*, **1107**, 166.

685 Kinny, P. D., Friend, C. R. L., Strachan, R. A., Watt, G. R., & Burns, I. M. 1999. U–Pb geochronology of
686 regional migmatites in East Sutherland, Scotland: evidence for crustal melting during the
687 Caledonian orogeny. *Journal of the Geological Society*, **156**(6), 1143-1152.

688 Kinny, P.D., Friend, C.R.L. & Love, G.J. 2005. Proposal for a terrane-based nomenclature for the
689 Lewisian Gneiss Complex of NW Scotland. *Contributions to Mineralogy and Petrology*, **162**, 175-
690 186.

691 Kirkland, C.L., Bingen, B., Whitehouse, M.J., Beyer, E. & Griffin, W.L. 2011. Neoproterozoic
692 palaeogeography in the North Atlantic Region: Inferences from the Akkajaure and Seve Nappes in
693 the Scandinavian Caledonides. *Precambrian Research*, **186**, 127-146.

694 Košler, J., Forst, L. & Sláma, J. 2008. LamDate and LamTool: Spreadsheet-based data reduction for laser
695 ablation ICP-MS. In: *Sylvester, P.J. (ed) Laser ablation in the Earth Sciences: Current practices*
696 *and outstanding issues. Short Course Series, 40*, Mineralogical Association of Canada, Quebec,
697 315-317.

698 Lambert, R.S., & McKerrow, W.S. 1976 The Grampian Orogeny. *Scottish Journal of Geology*, **12**, 271-
699 292

700 Leslie, A.G., Smith, M. & Soper, N.J. 2008. Laurentian margin evolution and the Caledonian orogeny – a
701 template for Scotland and East Greenland. *In*: Higgins, A.K., Gilotti, J.A. & Smith, M.P. (eds) *The*
702 *Caledonides of Greenland: Evolution of the Northeast Margin of Laurentia*. Geological Society of
703 America Memoir, **202**, 307-343.

704 Leslie, A.G., Robertson, S., Smith, M., Banks, C.J., Mendum, J.R., & Stephenson, D. 2013. The Dalradian
705 rocks of the northern Grampian Highlands of Scotland. *Proceedings of the Geologists' Association*,
706 **124**(1), 263-317.

707 Love, G. J., Kinny, P. D., & Friend, C. R. L. 2004. Timing of magmatism and metamorphism in the
708 Gruinard Bay area of the Lewisian Gneiss Complex: comparisons with the Assynt Terrane and
709 implications for terrane accretion. *Contributions to Mineralogy and Petrology*, **146**(5), 620-636.

710 Ludwig, K.R., 2003. *Isoplot 3.00. A geochronological toolkit for Microsoft Excel.* Berkeley
711 Geochronology Center, Berkeley, CA special publication no. 4a, 70

712 Ludwig, K.R. 2009. *Squid II, a user's manual*. Berkley Geochronology Center, Berkley, CA Special
713 Publication no. 2

714 Lundmark, A.M., Sæther, T. & Sørlie, R. 2014. Ordovician to Silurian magmatism on the Ultsira High,
715 North Sea: implications for correlations between the onshore and offshore Caledonides. *In*:
716 Corfu, F., Gasser, D. & Chew, D. (eds) *New Perspectives on the Caledonides of Scandinavia*.
717 Geological Society, London, Special Publications, **390**, 513-523

718 Malone, S. J., McClelland, W. C., Werner von, G. & Piepjohn, K. 2014. Proterozoic Evolution of the
719 North Atlantic–Arctic Caledonides: Insights from Detrital Zircon Analysis of Metasedimentary
720 Rocks from the Pearya Terrane, Canadian High Arctic. *Journal of Geology*, **122**, 623-647.

721 McBride, J. H., & England, R. W. 1994. Deep seismic reflection structure of the Caledonian orogenic
722 front west of Shetland. *Journal of the Geological Society, London,* **151**(1), 9-16.

723 Moorhouse, S.J. & Moorhouse, V.E. 1988. The Moine Assemblage in Sutherland. *In*: Winchester, J.A.
724 (ed.) *Later Proterozoic Stratigraphy in the Northern Atlantic Regions*. Blackie, Glasgow, 54-73.

725 Moyen, J.F. & Martin, H. 2012. Forty years of TTG research. *Lithos*, **148**, 312-336.

726 Nasdala, L., Zhang, M., Kempe, U., Panczer, G., Gaft, M., Andrut, M., & Plötze, M. 2003. Spectroscopic
727 methods applied to zircon. *Reviews in Mineralogy and Geochemistry*, **53**(1), 427-467.

728 Nasdala, L., Hanchar, J.M., Kronz, A. & Whitehouse, M.J. 2005. Long-term stability of alpha particle
729 damage in natural zircon. *Chemical Geology*, **220**, 83-103.

730 Nutman, A.P. & Collerson, K.D. 1991. Very early Archean crustal-accretion complexes preserved in the
731 North Atlantic Craton. *Geology*, **19**, 791-794.

732 Nutman, A.P., Friend, C.R., & Hiess, J. 2010. Setting of the∼ 2560 Ma Qôrqut Granite complex in the
733 archean crustal evolution of southern west Greenland. *American Journal of Science*, **310**(9), 1081-
734 1114.

735 Oliver, G. J. H., Chen, F., Buchwaldt, R., & Hegner, E. 2000. Fast tectonometamorphism and exhumation
736 in the type area of the Barrovian and Buchan zones. *Geology*, **28**(5), 459-462.

737 Peach, B.N., Horne, J., Woodward, H.B., Clough, C.T., Harker, A. & Wedd, C.D. 1910. *The Geology of*
738 *Glenelg, Lochalsh and south-east part of Skye.* Memoirs of the Geological Survey of Great Britain.

739 Pickering, K.T., Bassett, M.G., & Siveter D.J. 1988. Late Ordovician–early Silurian destruction of the
740 Iapetus Ocean: Newfoundland, British Isles and Scandinavia—a discussion. Transactions of the
741 Royal Society of Edinburgh. *Earth Sciences,* **79**(4), 361-382.

742 Ramsay, J.G. 1958. Moine-Lewisian relations at Glenelg, Inverness-shire. *Quarterly Journal of the*
743 *Geological Society of London,* **113,** 487-523.

744 Ramsay, J.G. 1963. Structure and metamorphism of the Moine and Lewisian rocks of the North-West
745 Caledonides. *In*: Johnson, M.R.W. & Stewart, F.H. (eds). *The British Caledonides*. Oliver & Boyd,
746 Edinburgh, 143-170.

747 Ritchie, J. D., Hitchen, K., & Mitchell, J. G. 1987. The offshore continuation of the Moine Thrust north of
748 Shetland as deduced from basement isotopic ages. *Scottish Journal of Geology,* **23**(2), 163-173.

749 Robinson, T. 1983. Basement/cover relations in West Shetland. Unpublished Ph.D. Thesis, University of
750 Liverpool

751 Rogers, G., Hyslop, E. K., Strachan, R. A., Paterson, B. A., & Holdsworth, R. E. 1998. The structural
752 setting and U–Pb geochronology of Knoydartian pegmatites in W Inverness-shire: evidence for
753 Neoproterozoic tectonothermal events in the Moineof NW Scotland. *Journal of the Geological*
754 *Society, London,* **155**(4), 685-696.

755 Rollinson, H.R. & Fowler, M.B. 1987. The magmatic evolution of the Scourian Complex at Gruinard Bay.
756 *In*: Park, R.G. & Tarney, J. (eds) *The Evolution of the Lewisian and comparable high-grade*
757 *metamorphic terrains.* Geological Society, Special Publications, **27**, 57-71.

758 Slama, J. Košler, D.J. Condon, J.L. Crowley, A. Gerdes, J.M. Hanchar, M.S.A. Horstwood, G.A. Morris,
759 L. Nasdala, N. Norberg, U. Schaltegger, B. Schoene, M.N. Tubrett & M.J. Whitehouse. 2008.
760 Plešovice zircon – a new natural reference material for U-Pb and Hf isotopic microanalysis.
761 *Chemical Geology*, **249**, 1–35

762 Soper, N. J., Strachan R.A., Holdsworth R. E., Gayer R. A., & Greiling R. O. 1992. Sinistral transpression
763 and the Silurian closure of Iapetus. *Journal of the Geological Society, London,* **149**(6), 871-880.

764 Stern, R. & Amelin, Y. 2003. Assessment of errors in SIMS zircon U-Pb geochronology using a natural
765 zircon standard and NIST SRM 620 glass, *Chemical Geology.* **197**, 111-142.

766 Stern, R.A., Bodorkus, S., Kamo, S.L., Hickman, A.H., & Corfu, F. 2009. Measurement of SIMS
767 instrumental mass fractionation of Pb isotopes during zircon dating. *Geostandards and*
768 *Geoanalytical Research*, **33**(2), 145-168.

769 Storey, C. 2008. The Glenelg-Attadale Inlier, NW Scotland, with emphasis on the Precambrian high-
770 pressure metamorphics history and subsequent retrogression: an introduction and review. *Scottish*
771 *Journal of Geology*, **44**, 1-16

772 Strachan, R.A. & Holdsworth, R.E. 1988. Basement-cover relationships and structure within the Moine
773 rocks of central and southeast Sutherland. *Journal of the Geological Society, London,* **145,** 23-36.

774 Strachan, R. A., Smith, M., Harris, A. L., & Fettes, D. J. 2002. *The Northern Highland and Grampian*
775 *terranes. The Geology of Scotland*. Geological Society London, 81-147.

776 Strachan, R. A., Prave, A. R., Kirkland, C. L., & Storey, C. D. 2013. U-Pb detrital zircon geochronology
777 of the Dalradian Supergroup, Shetland Islands, Scotland: implications for regional correlations
778 and Neoproterozoic-Palaeozoic basin development. *Journal of the Geological Society*, *London*,
779 **170**, 905-916.

780 Tanner, P.W.G. 2013. A kinematic model for the Grampian Orogeny,Scotland. *In:* Corfu, F. Gasser, D., &
781 Chew, D.M. (eds) *New Perspectives on the Caledonides of Scandinavia and Related Areas.*
782 Geological Society, London, Special Publications, 390.

783 Tappe, S., Smart, K.A., Pearson, D.G., Steenfelt, A., & Simonetti, A. 2011. Craton formation in Late
784 Archean subduction zones revealed by first Greenland eclogites. *Geology*, **39**(12), 1103-1106.

785 Taylor, S.R. & McLennan, S.M. 1985. *The continental crust: its composition and evolution*. Blackwell,
786 Oxford, 312pp.

787 Taylor, R., Clark, C., Reddy, S.M. 2012. The effect of grain orientation on secondary ion mass
788 spectrometry (SIMS) analysis of rutile. *Chemical Geology,* **300**, 81-87.

789 Vance, D., Strachan, R. A., & Jones, K. A. 1998. Extensional versus compressional settings for
790 metamorphism: Garnet chronometry and pressure-temperature-time histories in the Moine
791 Supergroup, northwest Scotland. *Geology*, **26**(10), 927-930.

792 Walker, S, Thirlwall, M.F., Strachan, R.A., & Bird, A.F. 2016. Evidence from Rb-Sr mineral ages for
793 multiple orogenic events in the Caledonides of Shetland, Scotland. *Journal of the Geological*
794 *Society, London*, in press.

795 Wheeler, J., Park, R.G., Rollinson, H. R., & Beach, A. 2010. The Lewisian Complex: insights into deep
796 crustal evolution. *In*: Law, R.D., Butler, R.W.H., Holdsworth, R.E., Krabbendam, M. & Strachan,
797 R.A. (eds) Continental Tectonics and Mountain Building – The Legacy of Peach and Horne.
798 *Geological Society, London, Special Publications*, **335**(1), 51-79.

799 Williams, I.S. 1998. U–Th–Pb geochronology by ion microprobe, in Applications of Microanalytical
800 Techniques to Understanding Mineralizing Processes edited by MA McKibben, WC Shanks III, and
801 WI Ridley. *Reviews in Economic Geology*, **7**, 1–35.

802 Winchester, J.A. & Lambert, R.St.J. 1970. Geochemical distinctions between the Lewisian of Cassley,
803 Durcha and Loch Shin, Sutherland and the surrounding Moinian. *Proceedings of the Geologists'*
804 *Association*, **81,** 275-301.

805

Figures:

Fig.1. (**a**) Location of Shetland in the British Isles. Box indicates location of (b). Abbreviations: B, Bute; GGF, Great Glen Fault; HBF, Highland Boundary Fault; HT, Hebridean Terrane; IS, Iapetus Suture; MVT, Midland Valley Terrane; GT, Grampian Terrane; MT, Moine Thrust; NHT, Northern Highland Terrane; SUF, Southern Uplands Fault; WBF, Walls Boundary Fault; WKSZ, Wester Keolka Shear Zone. (b) Simplified geological map of the northern part of Shetland (modified after Cutts et al. 2009), the study area in northeast Yell is enclosed in a box. Abbreviations: BMF, Bluemull Sound Fault; BFL, Burra Firth Lineament; H, Hascosay; WKSZ, Wester Keolka Shear Zone.

Fig. 2. Geological sketch map of northeast Yell, showing the trends of foliation and lineation in the region, and sample locations.

Fig. 3. (**a-b**) Photographs of the basement gneisses south of Bay of Brough. (**c**) Photograph of sample SH12-04, garnet bearing metagabbro (**d**) Photograph from the SH12-09 sample locality at Migga Ness showing the strongly lineated orthogneiss.

Fig. 4. (**a**) CL images of representative zircons from sample SH12-04 (metagabbro). (**b**) CL images of representative zircons from sample SH12-14 (paragneiss, YSG). (**c**) CL images of representative zircons from sample SH12-16 (orthogneiss). SHRIMP analytical sites are shown as circles together with site number and the indicated U-Pb age in Ma, ($^{207}Pb/^{206}Pb$ ages are quoted if older than 1.2 Ga, and $^{206}Pb/^{238}U$ ages if younger, with 1σ errors).

Fig. 5. (**a-d**) CL images of representative zircons from orthogneiss sample 11CL-02. (**e-h**) CL images of representative zircons from orthogneiss sample 11CL-04. LA-ICPMS analytical sites are shown as raster lines together with site number and the indicated U-Pb age in Ma, ($^{207}Pb/^{206}Pb$ ages are quoted if older than 1.2 Ga, and $^{206}Pb/^{238}U$ ages if younger, with 1σ errors).

Fig. 6. Error ellipses shown at 2σ level. (**a**) Concordia diagram showing the results of all zircon analyses for sample SH12-04. (**b**) Concordia diagram showing the results of all zircon analyses for sample SH12-09. (**c**) Concordia diagram showing the results of zircon analyses for sample SH12-16, 3 analyses with large errors have been omitted (**d**) Concordia diagram showing the subset of results of younger zircon with <10% discordance for sample SH12-16. (**e**) Concordia diagram showing the subset of results of zircon with <10% discordance for sample SH12-14. (**f**) Concordia diagram showing the subset of younger zircon with <10% discordance for sample SH12-14 colour coded according to Th/U ratio.

Fig. 7. (**a**) Concordia diagram showing the results of all zircon analyses for sample 11CL-02. (**b**) Concordia diagram showing the younger population of zircon analyses for sample 11CL-02. (**c**) Concordia diagram showing the results of all zircon analyses for sample 11CL-04. (**d**) Concordia diagram showing the younger population of zircon analyses for sample 11CL-04.

Fig. 8. Concordia diagram showing the results of rutile analyses for sample SH12-14 (analyses with large errors have been omitted).

Fig. 9. Harker variation diagrams for major and trace elements in mafic (solid symbols) and felsic (open symbols) samples of the Cullivoe gneisses.

Fig. 10. Total alkalis versus silica diagram showing data from the mafic (solid symbols) and felsic (open symbols) samples of the Cullivoe gneisses.

Fig. 11. (**a**) Ab - An - Or diagram showing data from the felsic Cullivoe gneisses. (**b**) AFM diagram showing data from the mafic (solid symbols) and felsic (open symbols) samples of the Cullivoe gneisses.

Fig. 12. Chondrite-normalised REE plots showing data from the mafic (solid symbols) and felsic (open symbols) samples of the Cullivoe gneisses.

Figure 1

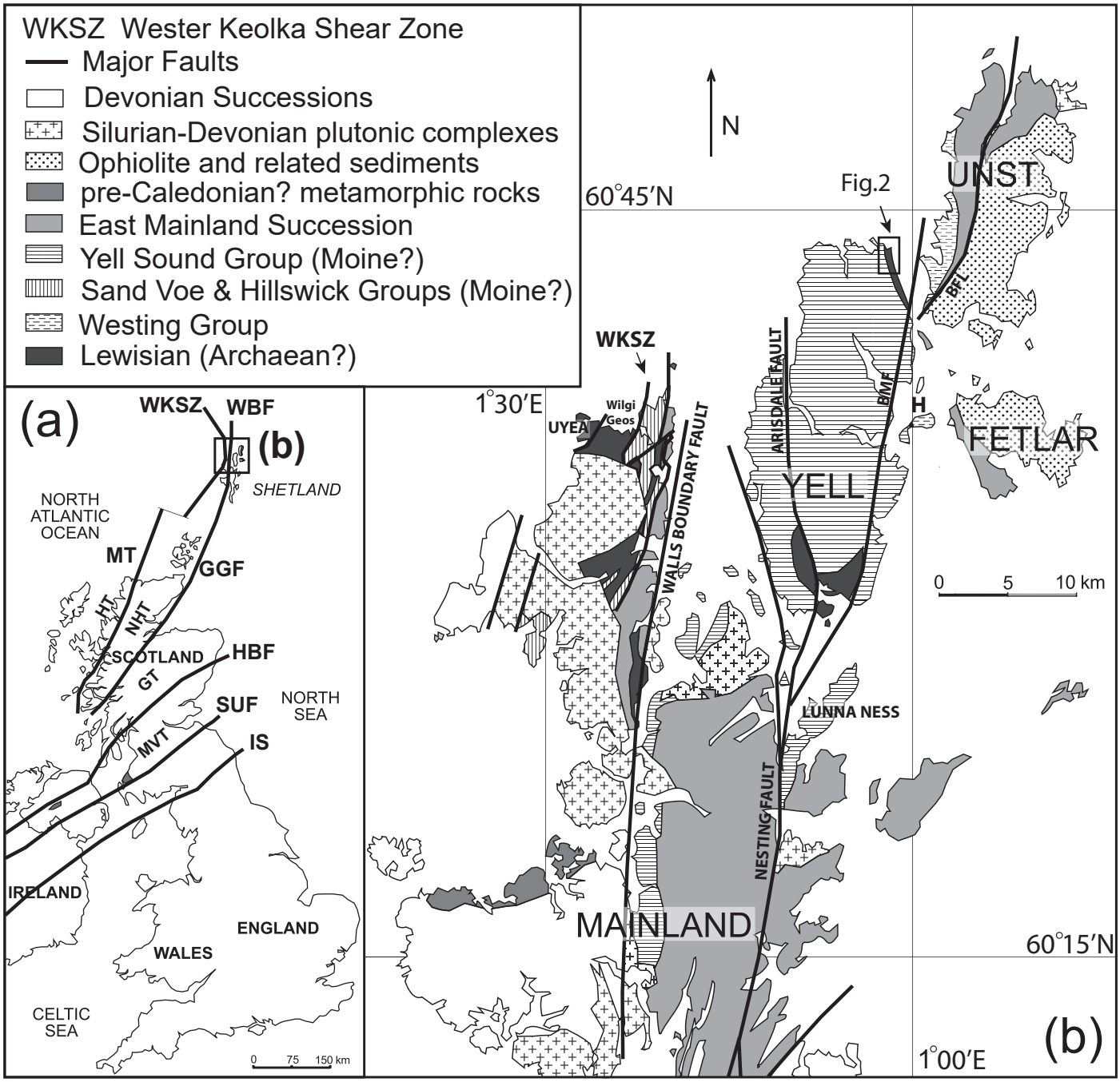
WKSZ Wester Keolka Shear Zone
Major Faults
Devonian Successions
Silurian-Devonian plutonic complexes
Ophiolite and related sediments
pre-Caledonian? metamorphic rocks
East Mainland Succession
Yell Sound Group (Moine?)
Sand Voe & Hillswick Groups (Moine?)
Westing Group
Lewisian (Archaean?)
(a)
WKSZ
WBF
(b)
SHETLAND
NORTH ATLANTIC OCEAN
MT
GGF
HT
NHT
SCOTLAND
HBF
GT
SUF
NORTH SEA
MVT
IS
IRELAND
ENGLAND
WALES
CELTIC SEA
0 75 150 km
N
60°45′N
Fig.2
UNST
BFL
WKSZ
1°30′E
Wilgi Geos
UYEA
WALLS BOUNDARY FAULT
ARISDALE FAULT
BMF
H
FETLAR
YELL
0 5 10 km
LUNNA NESS
NESTING FAULT
MAINLAND
60°15′N
1°00′E
(b)

Figure 2

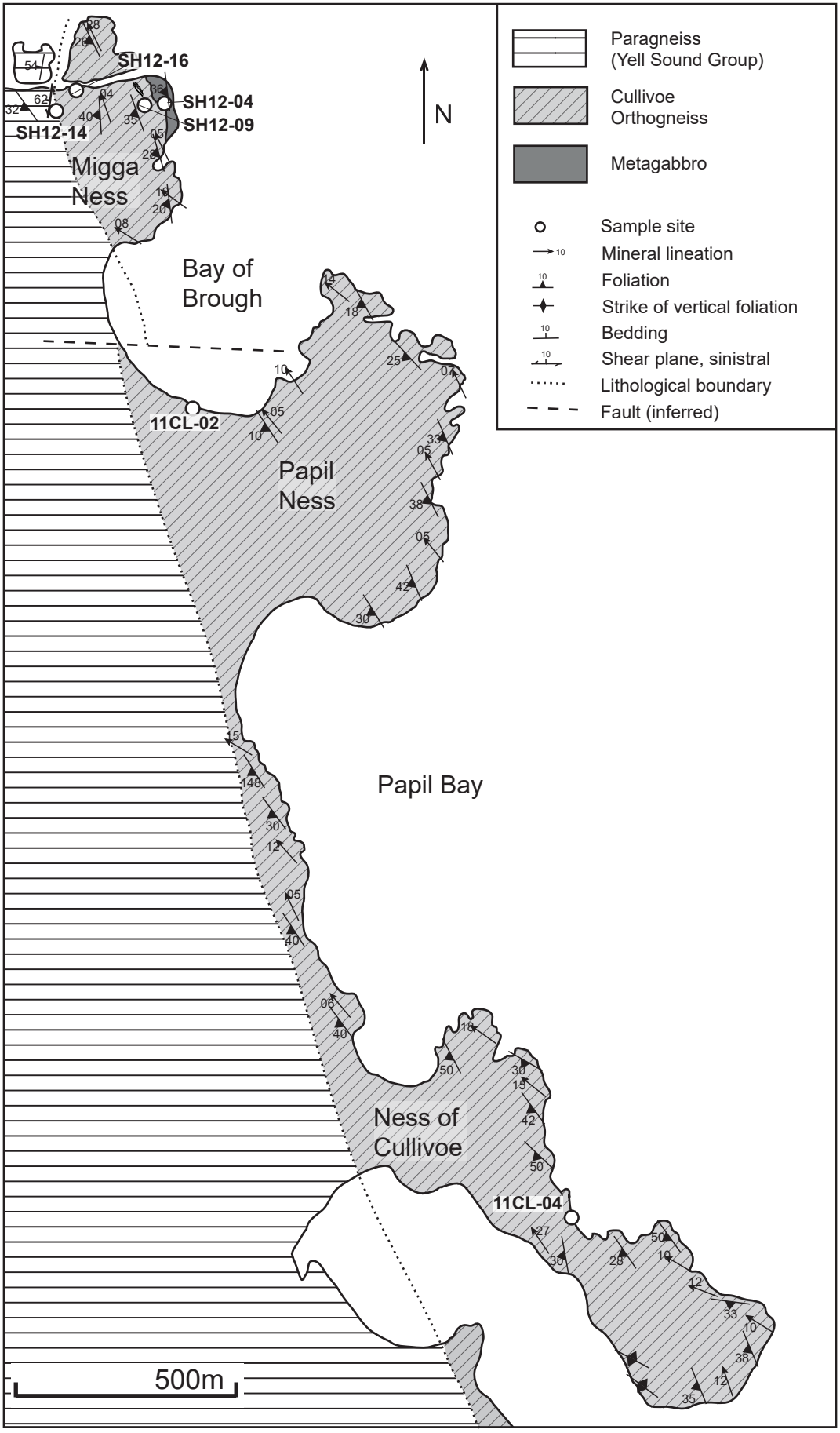
Paragneiss
(Yell Sound Group)
Cullivoe
Orthogneiss
Metagabbro
Sample site
Mineral lineation
Foliation
Strike of vertical foliation
Bedding
Shear plane, sinistral
Lithological boundary
Fault (inferred)
N
SH12-16
SH12-04
SH12-09
SH12-14
Migga
Ness
Bay of
Brough
11CL-02
Papil
Ness
Papil Bay
Ness of
Cullivoe
11CL-04
500m

Figure 3

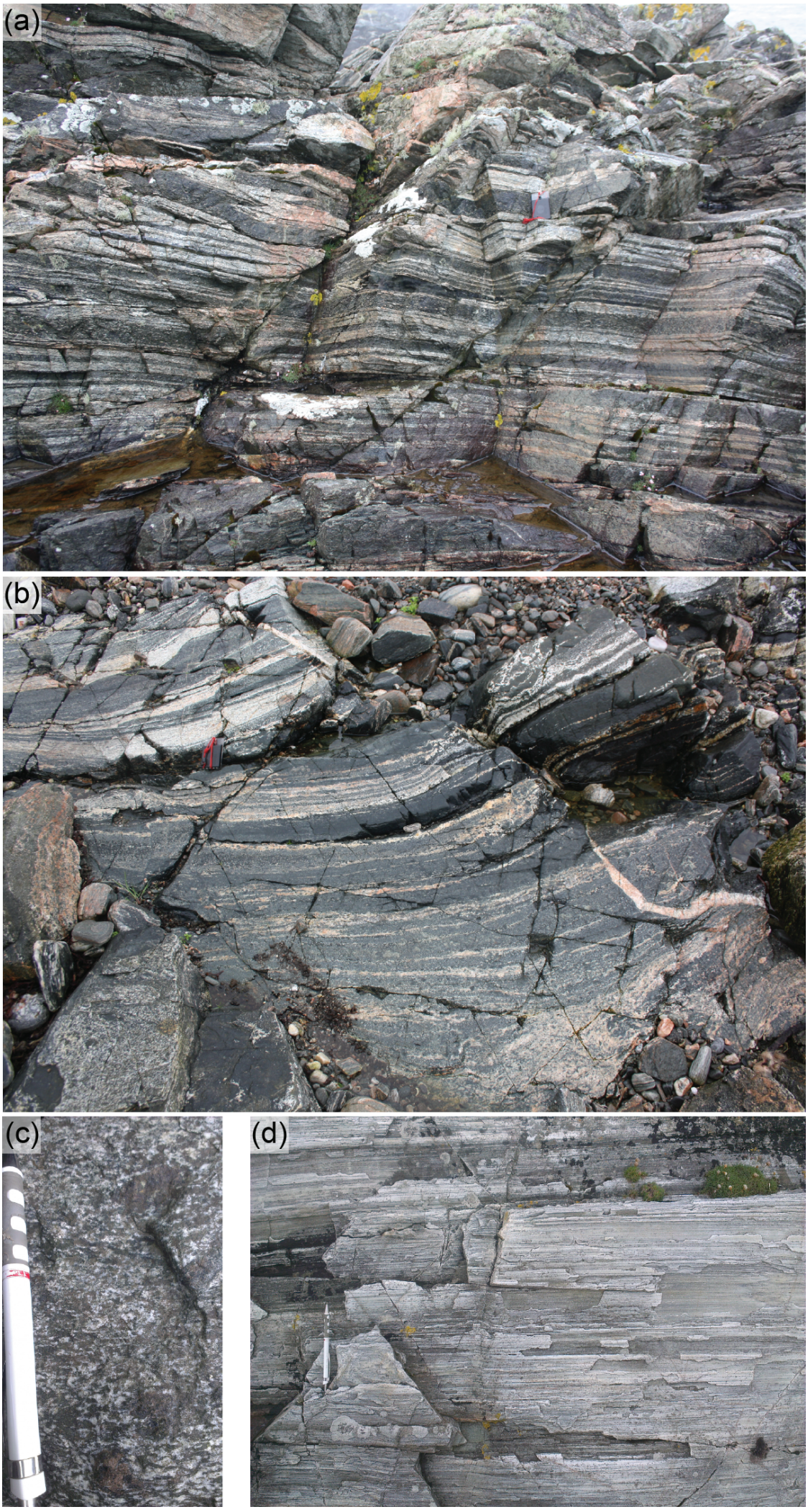

Figure 4

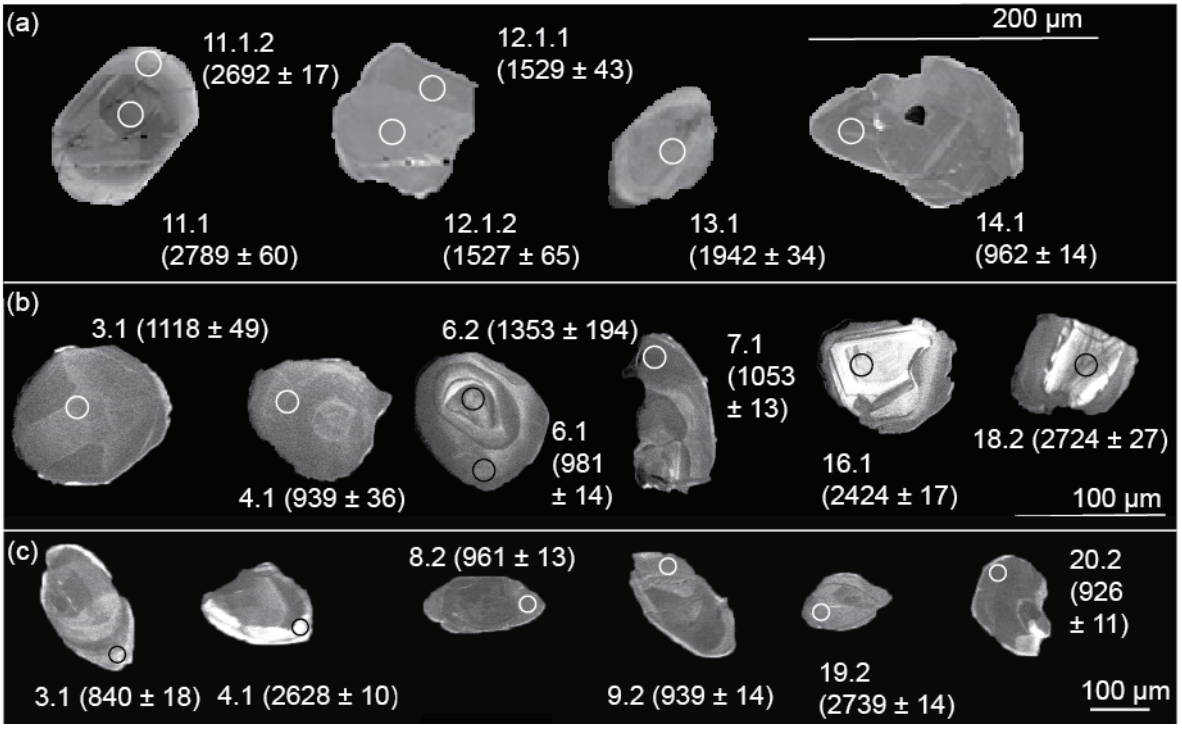
(a)
200 µm
11.1.2
(2692 ± 17)
12.1.1
(1529 ± 43)
11.1
(2789 ± 60)
12.1.2
(1527 ± 65)
13.1
(1942 ± 34)
14.1
(962 ± 14)
(b)
3.1 (1118 ± 49)
6.2 (1353 ± 194)
7.1
(1053
± 13)
6.1
(981
± 14)
18.2 (2724 ± 27)
16.1
(2424 ± 17)
4.1 (939 ± 36)
100 µm
(c)
8.2 (961 ± 13)
20.2
(926
± 11)
3.1 (840 ± 18)
4.1 (2628 ± 10)
9.2 (939 ± 14)
19.2
(2739 ± 14)
100 µm

Figure 5

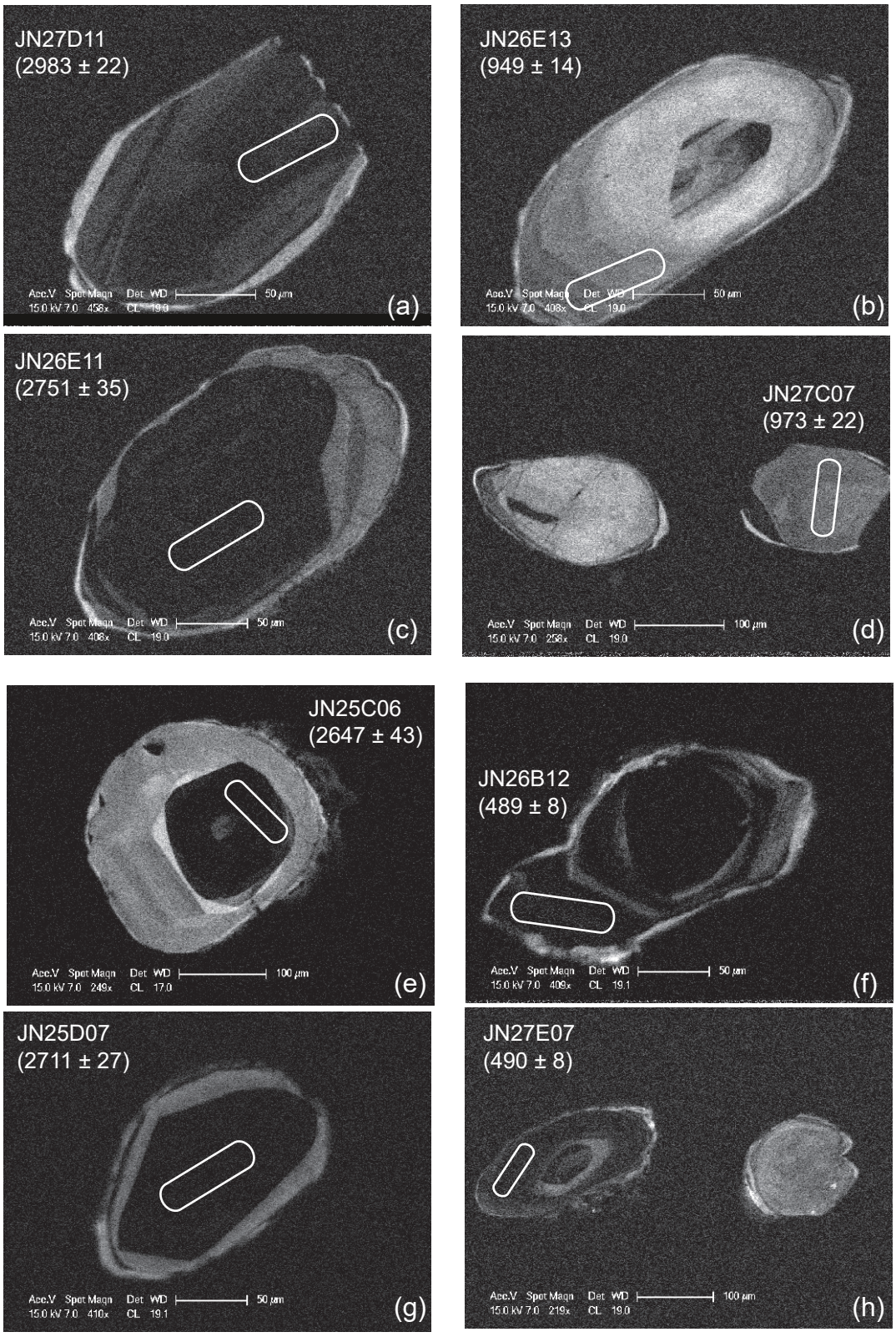
JN27D11
(2983 ± 22)
(a)
JN26E13
(949 ± 14)
(b)
JN26E11
(2751 ± 35)
(c)
JN27C07
(973 ± 22)
(d)
JN25C06
(2647 ± 43)
(e)
JN26B12
(489 ± 8)
(f)
JN25D07
(2711 ± 27)
(g)
JN27E07
(490 ± 8)
(h)

Figure 6

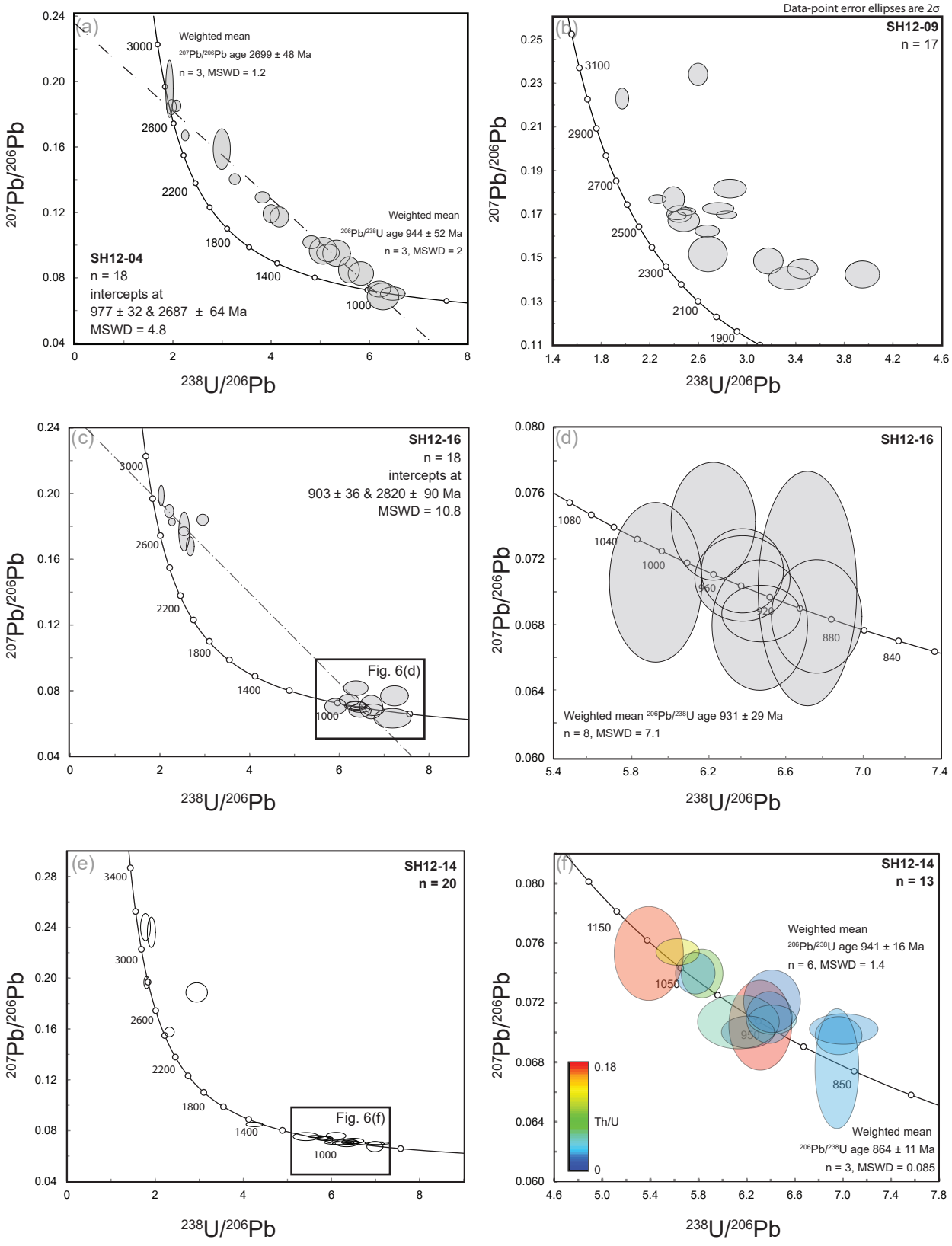
(a)
Weighted mean
$^{207}Pb/^{206}Pb$ age 2699 ± 48 Ma
n = 3, MSWD = 1.2
Weighted mean
$^{206}Pb/^{238}U$ age 944 ± 52 Ma
n = 3, MSWD = 2
SH12-04
n = 18
intercepts at
977 ± 32 & 2687 ± 64 Ma
MSWD = 4.8
(b)
Data-point error ellipses are 2σ
SH12-09
n = 17
(c)
SH12-16
n = 18
intercepts at
903 ± 36 & 2820 ± 90 Ma
MSWD = 10.8
Fig. 6(d)
(d)
SH12-16
Weighted mean $^{206}Pb/^{238}U$ age 931 ± 29 Ma
n = 8, MSWD = 7.1
(e)
SH12-14
n = 20
Fig. 6(f)
(f)
SH12-14
n = 13
Weighted mean
$^{206}Pb/^{238}U$ age 941 ± 16 Ma
n = 6, MSWD = 1.4
Th/U
Weighted mean
$^{206}Pb/^{238}U$ age 864 ± 11 Ma
n = 3, MSWD = 0.085
$^{207}Pb/^{206}Pb$
$^{238}U/^{206}Pb$

Figure 7

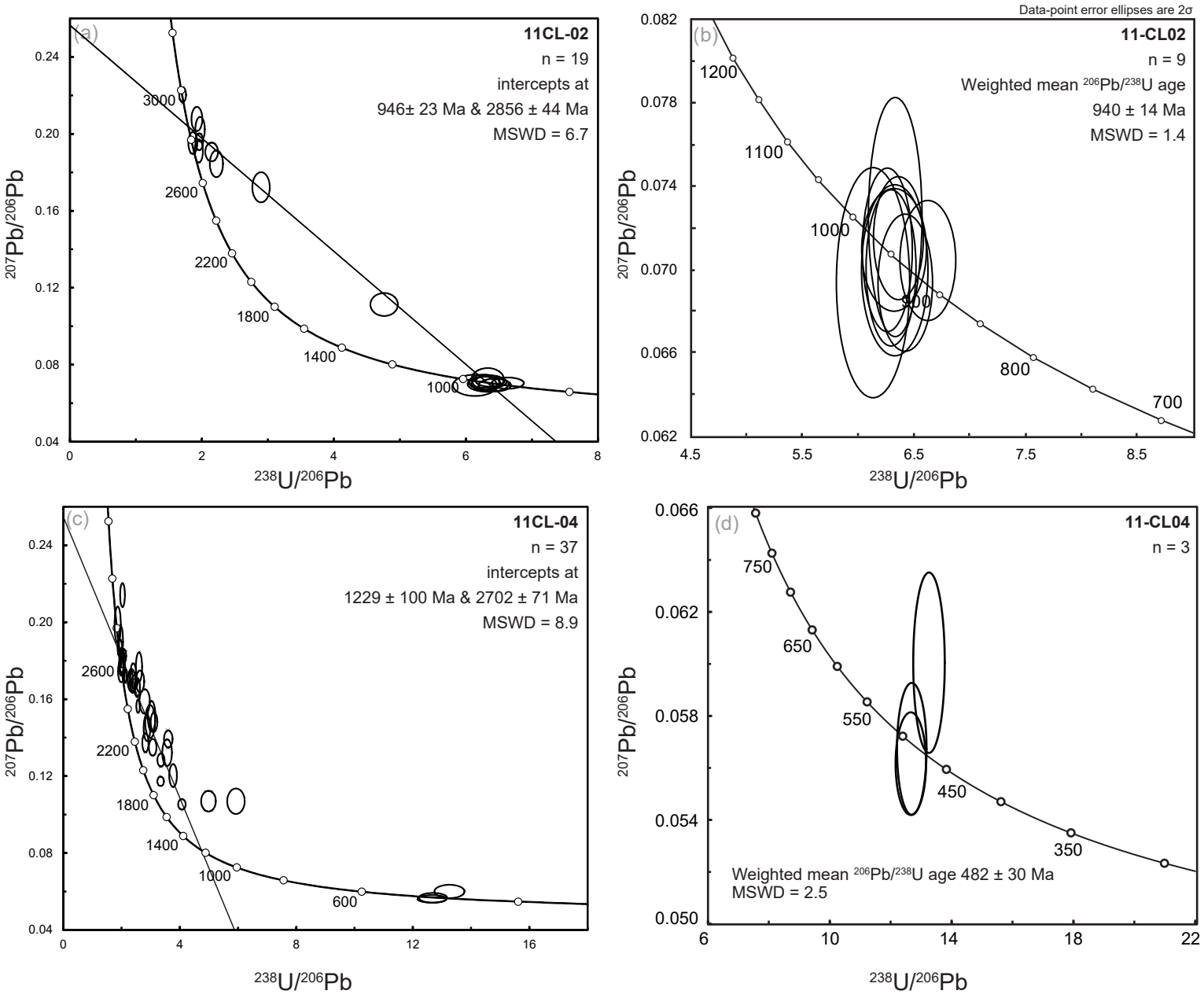
(a)
11CL-02
n = 19
intercepts at
946± 23 Ma & 2856 ± 44 Ma
MSWD = 6.7
3000
2600
2200
1800
1400
1000
$^{207}Pb/^{206}Pb$
$^{238}U/^{206}Pb$
Data-point error ellipses are 2σ
(b)
11-CL02
n = 9
Weighted mean $^{206}Pb/^{238}U$ age
940 ± 14 Ma
MSWD = 1.4
1200
1100
1000
900
800
700
(c)
11CL-04
n = 37
intercepts at
1229 ± 100 Ma & 2702 ± 71 Ma
MSWD = 8.9
2600
2200
1800
1400
1000
600
(d)
11-CL04
n = 3
750
650
550
450
350
Weighted mean $^{206}Pb/^{238}U$ age 482 ± 30 Ma
MSWD = 2.5

Figure 8

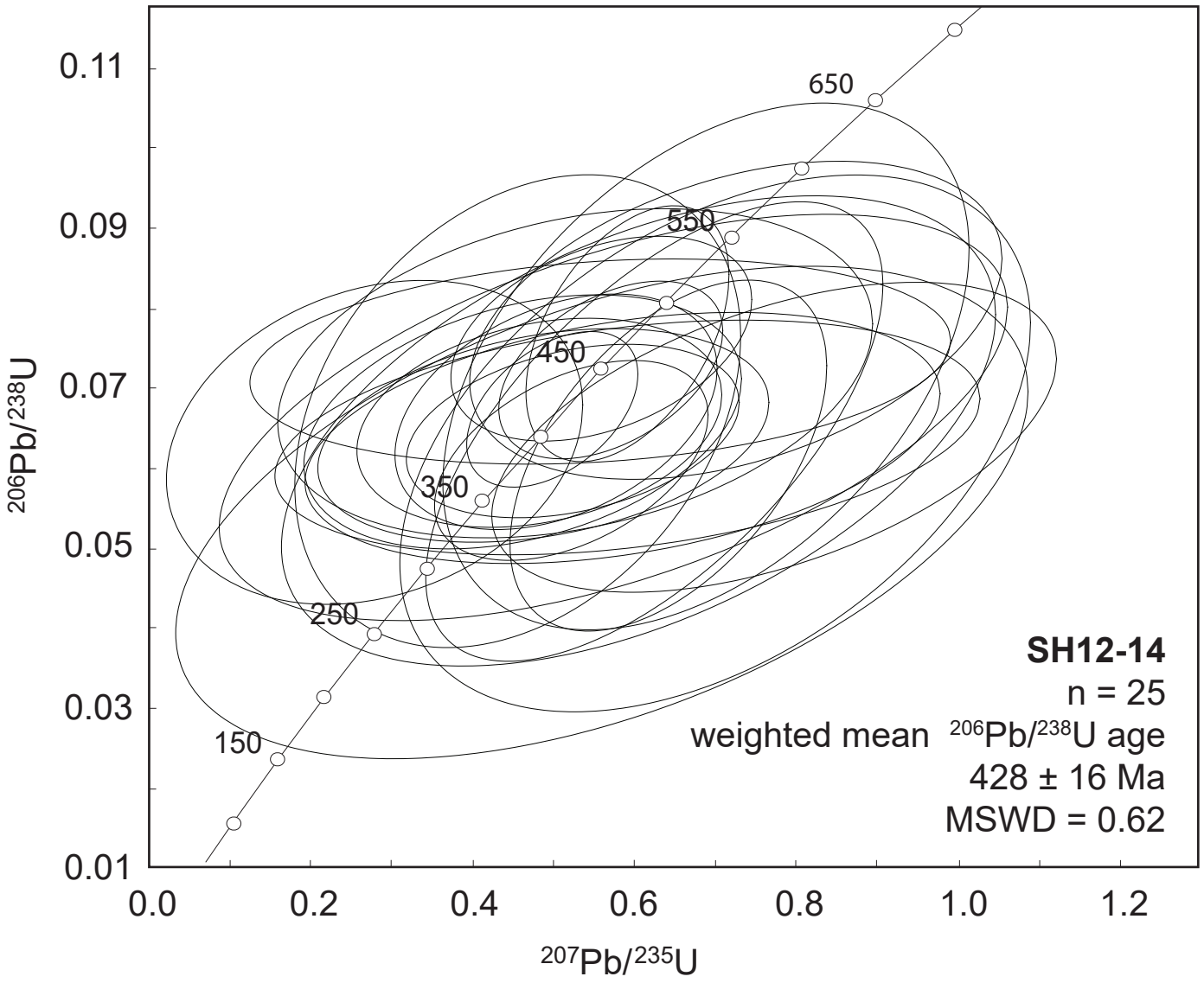
0.11
0.09
0.07
0.05
0.03
0.01
0.0
0.2
0.4
0.6
0.8
1.0
1.2
206Pb/238U
207Pb/235U
650
550
450
350
250
150
SH12-14
n = 25
weighted mean 206Pb/238U age
428 ± 16 Ma
MSWD = 0.62

Figure 9

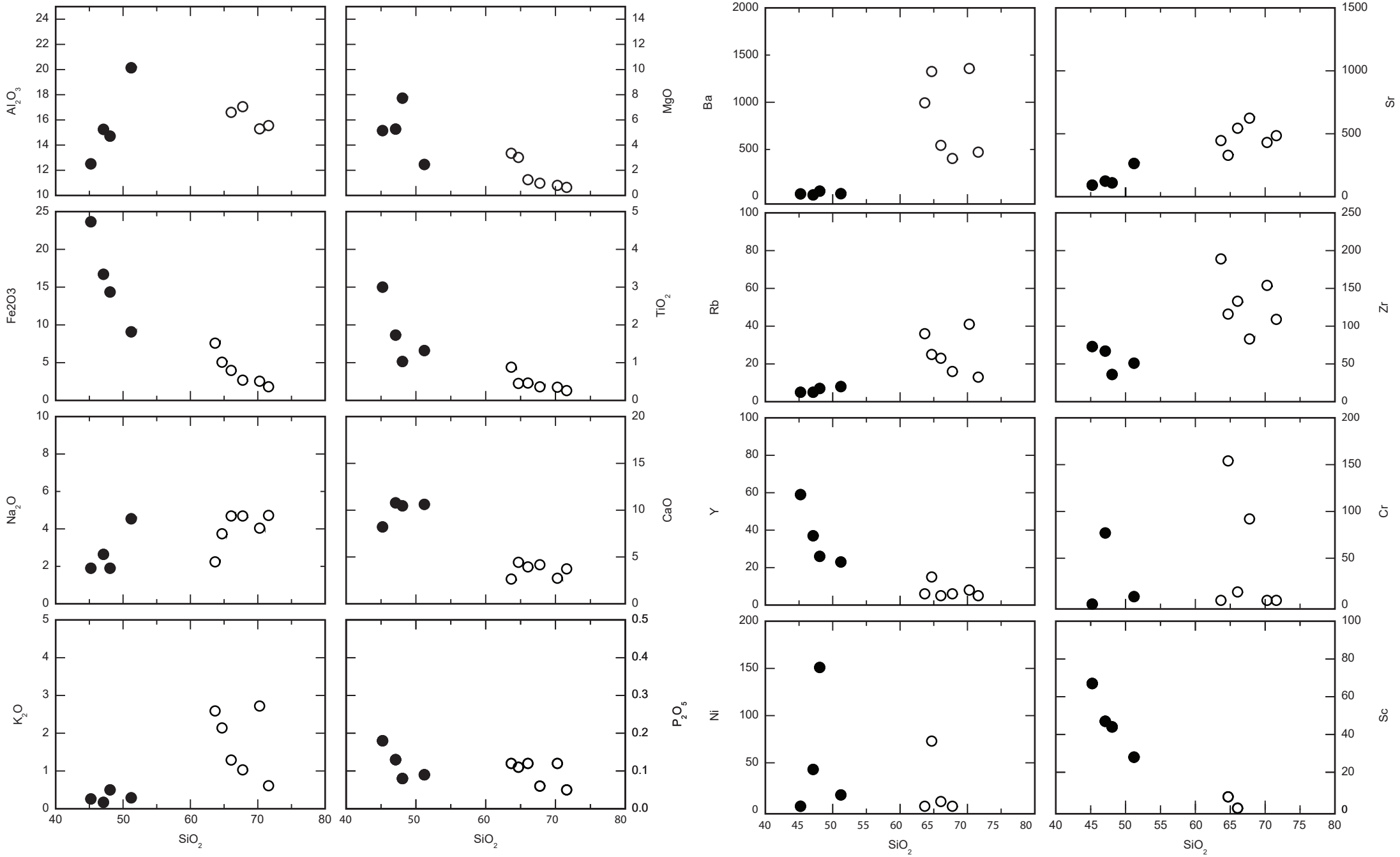
Al2O3
MgO
Fe2O3
TiO2
Na2O
CaO
K2O
P2O5
Ba
Sr
Rb
Zr
Y
Cr
Ni
Sc
SiO2
SiO2
SiO2
SiO2

Figure 10

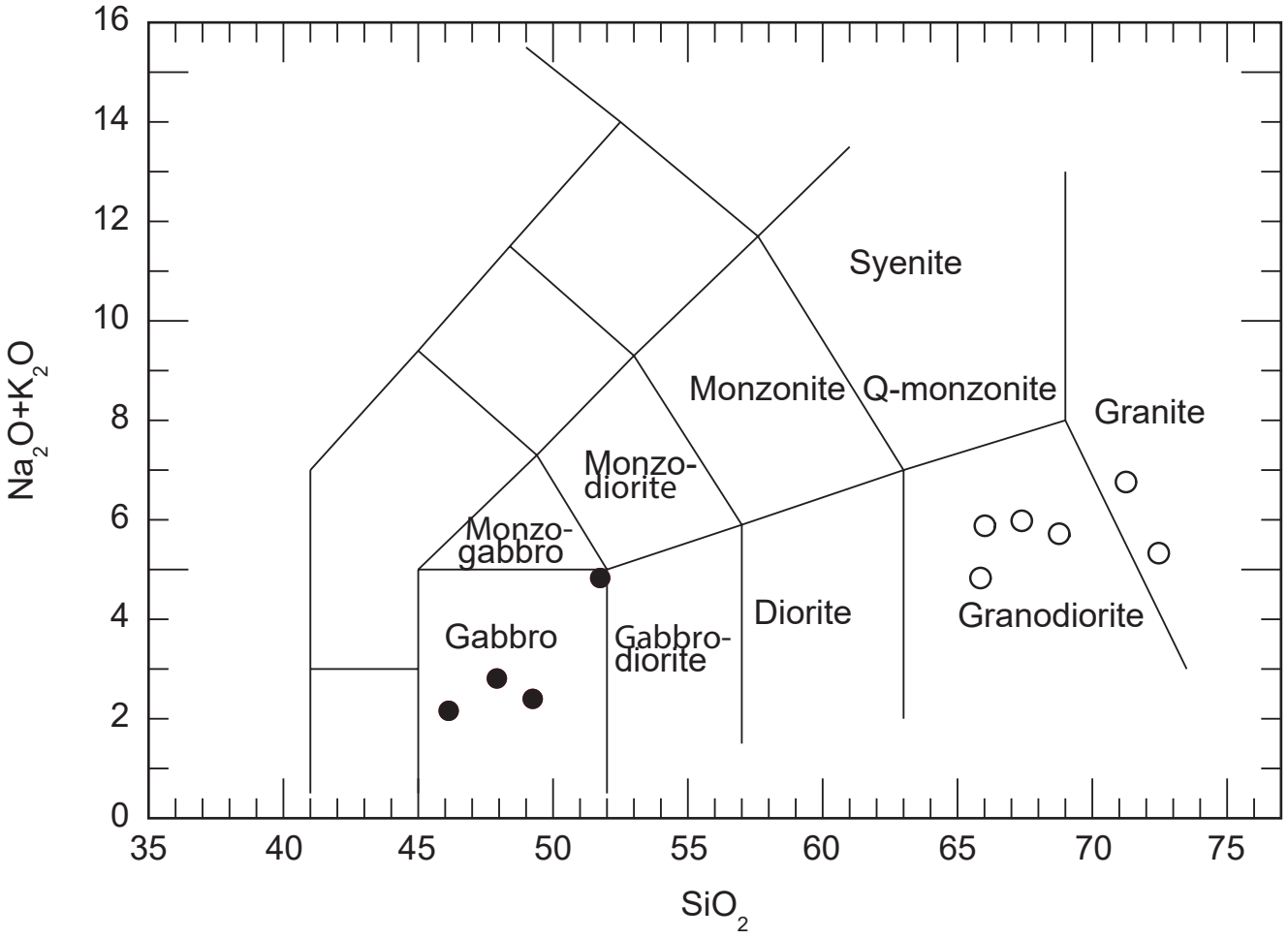
16
14
12
10
8
6
4
2
0
35
40
45
50
55
60
65
70
75
Na_2O+K_2O
SiO_2
Syenite
Monzonite
Q-monzonite
Granite
Monzo-
diorite
Monzo-
gabbro
Diorite
Granodiorite
Gabbro
Gabbro-
diorite

Figure 11

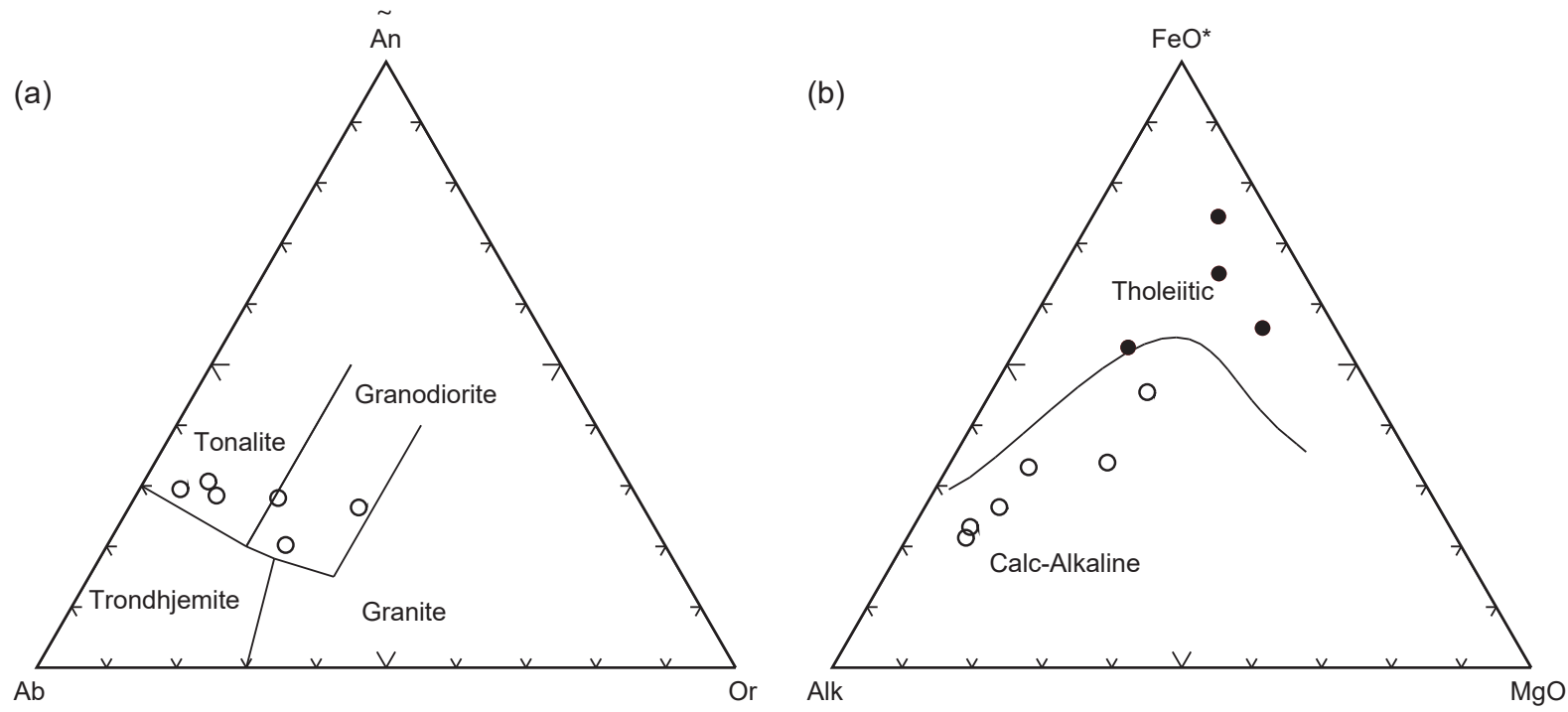
(a)
An
Granodiorite
Tonalite
Trondhjemite
Granite
Ab
Or
(b)
FeO*
Tholeiitic
Calc-Alkaline
Alk
MgO

Figure 12

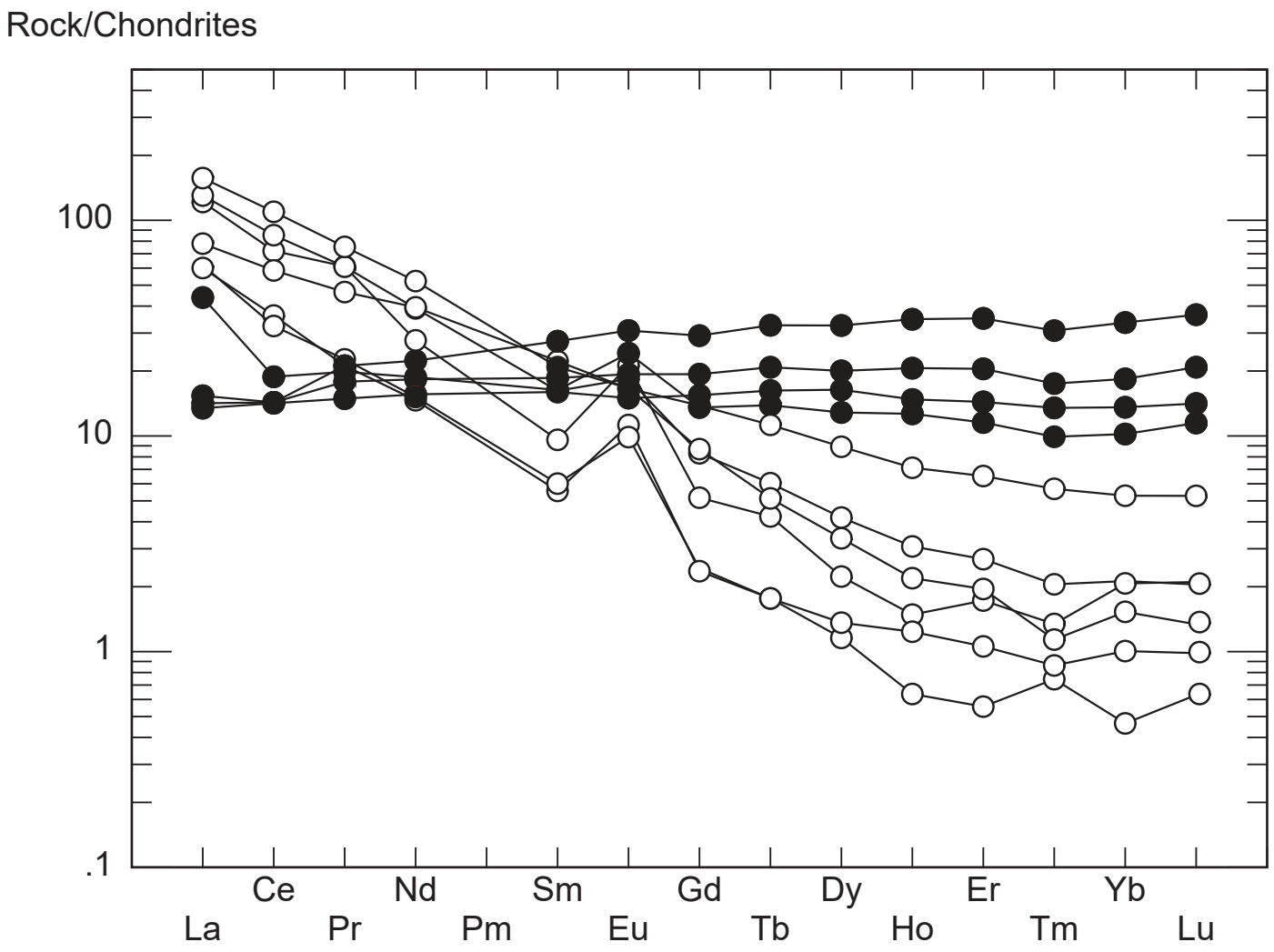
Rock/Chondrites
100
10
1
.1
La
Ce
Pr
Nd
Pm
Sm
Eu
Gd
Tb
Dy
Ho
Er
Tm
Yb
Lu